Preprints.org

Article

Not peer-reviewed version

RUL Prediction for LFP Batteries: Gompertz-Informed LSTMs for Enhanced Model Interpretability

Yuri Njathi * , Ciira wa Maina , Edwell T. Mharakurwa

Posted Date: 19 March 2026

doi: 10.20944/preprints202603.1540.v1

Keywords: battery health estimation; Remaining Useful Life; lithium-ion batteries; lithium iron phosphate batteries; LSTM; Gompertz model; hybrid modelling; physics-informed machine learning; State of Health; State of Charge; coulomb counting equation

Preprints.org is a free multidisciplinary platform providing preprint service that is dedicated to making early versions of research outputs permanently available and citable. Preprints posted at Preprints.org appear in Web of Science, Crossref, Google Scholar, Scilit, Europe PMC.

Copyright: This open access article is published under a Creative Commons CC BY 4.0 license, which permit the free download, distribution, and reuse, provided that the author and preprint are cited in any reuse.

Preprints.org (www.preprints.org) | NOT PEER-REVIEWED | Posted: 19 March 2026 doi:10.20944/preprints202603.1540.v1

Disclaimer/Publisher's Note: The statements, opinions, and data contained in all publications are solely those of the individual author(s) and contributor(s) and not of MDPI and/or the editor(s). MDPI and/or the editor(s) disclaim responsibility for any injury to people or property resulting from any ideas, methods, instructions, or products referred to in the content.

Article

RUL Prediction for LFP Batteries: Gompertz-Informed LSTMs for Enhanced Model Interpretability

Yuri Njathi [1,2,*], Ciira wa Maina [1,2] and Edwell.T. Mharakurwa [1]

[1] Department of Electrical and Electronic Engineering, Dedan Kimathi University of Technology, Dedan Kimathi, Nyeri P.O. Box 10143, Kenya

[2] Centre for Data Science and Artificial Intelligence (DSAIL), Dedan Kimathi University of Technology, Dedan Kimathi, Nyeri P.O. Box 10143, Kenya

* Correspondence: yuri.njathi@dkut.ac.ke

Abstract

Lithium iron phosphate batteries have seen a recent rise in usage in electric vehicles and battery energy storage systems. For these applications, reliability is of paramount importance and influences long-term adoption especially when replacing a used battery as it influences product warranties and consumer trust. Remaining Useful Life (RUL) prediction is at the core of avoiding unexpected failure and enabling proactive battery maintenance. Physics-based and data-driven methods have been explored by researchers, whilst Physics-Informed Neural Networks (PINNs) can combine their strengths in estimating battery RUL. This paper proposes Gompertz-Informed LSTMs (GILSTMs), approaches that combine the Gompertz function, an inherently interpretable white-box model, with LSTMs to capture both downward monotonic behaviour and long-term dependencies from data. LSTMs are regarded as black box systems and critical infrastructure operators may refrain from using such black box systems. Gray-box models such as GILSTMs may get over the hurdle by increasing model interpretability and chances of industrial adoption for battery energy storage systems, while also benefitting from data-driven modelling. This study explores two GILSTM architectures: the first uses an LSTM to predict Gompertz parameters, which are then converted into RUL via the inverse Gompertz equation. The second uses the inverse Gompertz equation as a verification step to cross-check the RUL values generated by the LSTM. The first type of GILSTM was constrained by both a physics loss and an inverse Gompertz layer to predict RUL while the second verified the results of an LSTM, despite that the GILSTMs failed to generalize. The first type of GILSTM achieved an average RMSE of 22.97%, while the second type achieved an average RMSE of 26.99%. The models in this paper are also benchmarked on the first 100 cycles, a current state of art for battery degradation testing. The best overall implementation was an LSTM that predicted RUL by recursively predicting SoH achieving an average RMSE per cycle of 9.18% and a 100th cycle RMSE of 17.02%.

Keywords: battery health estimation; Remaining Useful Life; lithium-ion batteries; lithium iron phosphate batteries; LSTM; Gompertz model; hybrid modelling; physics-informed machine learning; State of Health; State of Charge; coulomb counting equation

1. Introduction

An ideal power grid can match power supply and power demand by seamlessly balancing generation and consumption of power in real time. With the global rise in solar and wind sources, renewable and cheap energy is now more accessible. Unfortunately, solar and wind energy are intermittent, thus cannot be ramped up and down at will to match instantaneous electricity demand. Battery energy storage systems (BESSs) are poised to help wind and solar overcome this hurdle, increasing the cleanliness of many countries' energy grids as well as providing energy security to

© 2026 by the author(s). Distributed under a Creative Commons CC BY license.

Preprints.org (www.preprints.org) | NOT PEER-REVIEWED | Posted: 19 March 2026 doi:10.20944/preprints202603.1540.v1

millions of people. In Kenya, the power grid integrates various power sources such as geothermal, hydroelectric, wind, solar and thermal. Unfortunately, due to grid-attributed infrastructure failures, blackouts in Kenya have become very common even in the 2020s [1] reducing reliability and stability, interrupting residential and industrial work. Issues regarding power grid reliability may be exacerbated with the installation of data centres which are very sensitive to changes in power grid frequency [2–4]. Technologies such as pumped-hydro and lithium-ion batteries play a crucial role in storing excess energy and dispatching it when needed, reducing energy curtailment and providing support to maintaining the frequency of power-grids [5]. In Kenya, the System Average Interruption Duration Index (SAIDI) in the first half of the year 2024 was 11.45 hours per month [6], meaning on average every electricity customer of the 9.6 million electricity customers [7] in Kenya experiences 11.45 hours of power outage per month.

To address these blackout issues, many people are looking toward purchasing residential battery backup systems. KenGen, Kenya's largest electricity producer has proposed several BESS to be rolled out across Kenya between 2026 and 2041 with capacities of 2.2GW/4.7GWh, pending feasibility studies [8]. These batteries degrade over time and can cause unintended failures to occur if not managed properly. Knowing when to replace the batteries is crucial. This paper looks at understanding lithium iron phosphate (LFP) battery lifespan by providing an interpretable physics constrained framework for predicting the battery lifespans using Gompertz-Informed LSTM methods. The paper also addresses the potential implications and the ability of the method to follow physical degradation laws particularly the downward monotonic behaviour of LFP battery capacity degradation.

2. Background and Prior Work

This section details the technical and economic context for the research, beginning with a comparative analysis of energy storage technologies to highlight the advantages of Lithium-ion as a storage method. It then provides a detailed examination of the electrochemical properties and operational parameters related to LFP cells. This section builds up the necessary foundation to understand battery degradation mechanisms and the technical variables such as State of Health (SoH) and Remaining Useful Life (RUL) that are essential for the predictive modelling discussed later in this paper.

2.1. Batteries and Their Characteristics

There are over 60 types of batteries, one of which is the Lithium-ion battery (LiB) [9,10]. There are several chemistries within LiBs, the most prominent are lithium nickel manganese cobalt oxide (NMC), lithium nickel cobalt aluminium oxide (NCA) and lithium iron phosphate (LFP) batteries. In this paper, the focus is on the LFP batteries as they have recently eclipsed NMC and NCA batteries due to lower costs per kWh, thermal stability and safety [11].

Among the different types of batteries commonly used for grid-scale or consumer energy applications, the choice typically depends on key factors such as storage efficiency, energy density, lifespan, discharge duration, and peak power capacity. Table 1 outlines a detailed description of common battery types. LiBs have seen increasing adoption in small- and large-scale systems due to their growing practicability [12,13]. For instance, pumped hydro costs from $1700 to $5100 per kilowatt (on average $3400) while LiB systems are priced from $2500 to $3900 per kilowatt (on average $3200) [14] yet unlike LiB-based BESSs which can be deployed almost anywhere with varying scale depending on the use case, pumped hydro tends to require locations with two adjacent areas of low and high elevation (constrained by geography). In addition, pumped hydro implementations require very large capital costs, keeping pumped hydro out of reach for most people, organizations and some countries.

© 2026 by the author(s). Distributed under a Creative Commons CC BY license.

Preprints.org (www.preprints.org) | NOT PEER-REVIEWED | Posted: 19 March 2026 doi:10.20944/preprints202603.1540.v1

Table 1. Battery and their storage capacities.

Energy Storage Method	Max Power Rating (MW)	Discharge time	Max cycles or lifetime	Energy Density (Wh/liter)	Efficiency (%)
Pumped Hydro	3,000	4h – 16h	30-60 years	0.2-2	70-85
Li-ion	100	1 min – 8h	1000-10000 cycles	200-400	85-95
Lead-acid	100	1 min – 8h	6-40 years	50-80	80-90
Hydrogen	100	mins – week	5 – 30 years	600 (at 200 bar)	25-45
Flywheel	20	secs - mins	20,000 – 100,000 cycles	20-80	70-95

Beyond cost, LiBs offer advantages in terms of modularity and ease of development, especially in urban areas, where most electricity is used. LiB systems can be implemented at household, factory and grid levels; therefore, they are expected to play an increasingly large role in the transition to renewable, decarbonized energy systems. Due to these advantages of LiBs, their adoption in Kenya and many other countries would be of benefit to their respective power grid, especially regarding reducing SAIDI, integration of wind and solar energies, massively reducing the amount of grid energy that is curtailed and playing as a substitute to expensive fossil-fuel power plants.

2.2. Characteristics of LFP Batteries

Lithium Iron Phosphate batteries (LFPs) are a safer and a more thermally stable variant of lithium-ion batteries, known for their lower risk of thermal runaway [9–12], with a thermal runaway threshold ranging from 180°C - 250°C as seen in Table 2. LFPs typically offer a lifespan ranging from 1,000 to 10,000 charge-discharge cycles, which translates to approximately 2.74 to 27.4 years when used at a rate of one cycle per day. In 2024, LFPs accounted for approximately 40% to 59% of electric vehicle (EV) battery deployments and dominated the BESS market with an estimated 80% market share [13]. Their increasing popularity is driven by their durability, cost-effectiveness, and the elimination of critical materials like cobalt and nickel, making them more sustainable and geopolitically secure for large-scale energy storage and transportation applications [13].

The Remaining Useful Life (RUL) of LiBs refers to the number of charge-discharge cycles a battery can undergo while still maintaining an acceptable capacity. The definition of acceptable capacity is industrially defined as about 70-80% of its nominal capacity [14]. For example, an unused LFP battery with a nominal capacity of 1100 mAh may have a RUL ranging from 1000 to 10,000 cycles, depending on the manufacturer, operating conditions and usage. With each cycle, the battery undergoes gradual degradation, causing its capacity to decrease. When the capacity drops to 770mAh-880 mAh (70%-80% of 1100 mAh), the RUL reaches zero, signalling the end of its effective service life, thus a need for replacement.

The maximum capacity that the battery can draw at any point in time, relative to its capacity when new, is known as the State of Health (SoH). SoH is typically expressed as a percentage and serves as a real-time indicator of battery aging [14]. While RUL provides a forecast of how many more cycles a battery can deliver, SoH provides a snapshot of the battery's present condition, usage related properties such as those in Table 2 may inform the gradual change in SoH for LFP batteries. These two parameters, SoH and RUL, are closely related and are both critical in battery management systems (BMS) for ensuring safe operation, optimizing performance, and planning timely replacements in grid-scale and consumer applications. By monitoring the usage related properties of an LFP battery, with reference to those in Table 2, the SoH and RUL of an LFP battery can be estimated. The SoH values are fixed percentage points dependent on cycling conditions while the RUL varies greatly based on usage.

Battery users may usually be more concerned with the status of the battery within each charge-discharge cycle, the proportion of energy remaining in the battery relative to its nominal energy. This

© 2026 by the author(s). Distributed under a Creative Commons CC BY license.

Preprints.org (www.preprints.org) | NOT PEER-REVIEWED | Posted: 19 March 2026 doi:10.20944/preprints202603.1540.v1

proportion of energy remaining in a battery relative to its nominal energy is referred to as the State of Charge (SoC) and is usually indicated using a battery status bar or battery indicator; the nominal energy is a result of multiplying the nominal voltage with the nominal capacity and is expressed in Watt-hours (Wh) [15]. This SoC is typically expressed as a percentage ranging from 0% (fully discharged) to 100% (fully charged). If a battery is discharged below 0% SoC or charged beyond 100% SoC, irreversible chemical reactions may occur, leading to accelerated degradation and a significant drop in the SoH. Therefore, battery engineers have developed charging and discharging limits to properly approximate this SoC based on usage related properties as seen in Table 2.

One method for approximating SoC that has become very common for continuously operating battery systems is the Coulomb Counting (CC) method. The method is simple and standardized because it is accurate for short-term calculations [16]. The method uses the Coulomb Counting SoC estimation formula shown in Equation 1 [17,18]. Where $SoC\ (t_0)$ is the initial state of charge of the battery based on open circuit voltage or predictive means. C_{rated} is the nominal capacity of the battery/cell when it is new. I_{bat} is the battery current, t_0 is the initial time and t is the time when charging or discharging occurs. This equation simply calculates the area under the curve of current over time.

$$SoC(t) = SoC\ (t_0) + \frac{100\%}{C_{rated}} \int_{t0}^{t0+t} I_{bat}(\tau) d\tau \quad (1)$$

The coulomb counting equation doesn't directly address battery decay; thus, it can be erroneous due to long-term drift of the battery capacity from the rated capacity [16]. Enhanced coulomb counting methods have been proposed to address long term drift [19–21], each of which highlights the need to include battery decay by including the shift in SoH over time as shown in Equation (2).

$$SoC(t) = SoC\ (t_0) + \frac{100\%}{\mathrm{SoH} * \mathrm{C_{rated}}} \int_{t0}^{t0+t} I_{bat}(\tau) d\tau \quad (2)$$

This improvement is the integration of SoH into the traditional coulomb counting method used for State of Charge (SoC) estimation by accounting for the reduction in usable capacity over time can provide more accurate real-time SoC estimates. To achieve inclusion of SoH, causes of degradation need to be well understood. Charging above the maximum charge voltage can lead to overcharging, which has been found to accelerate degradation. Discharging below the minimum discharge voltage limit can result in over-discharge, leading to irreversible chemical changes that degrade the battery's capacity and potentially render the cell unusable. Higher speeds of discharging/charging of the cells relative to the nominal capacity (C-rate) increase internal resistance and thermal stress, leading to faster degradation. Studies show capacity fade correlates with cycles, temperature, and depth of discharge [22]. Proper estimation of SoC is usually employed to mitigate this degradation thus extending battery life. To control degradation, modern battery systems are equipped with a battery management system (BMS) that monitors and regulates SoC ensuring safe operation. SoC estimation has a direct influence on the SoH and the RUL of the battery, SoH estimation also has a direct influence on SoC and RUL. Accurate RUL prediction is essential for ensuring the reliability, safety and efficiency of battery-powered systems such as electric vehicles and renewable energy storage.

Table 2. Usage related properties of LFP Batteries.

Properties	Description
Nominal Voltage	3.2 volts [20]
Maximum Charge Voltage	3.65 V [21,22]
Minimum Discharge Voltage	2.0 V-2.8 V [23]
Charging rates	0.2-0.5 C [24]
Fast charge rate	1C [24]
Standard continuous discharging rate	1C [25]
High performance continuous discharging rate	2-3 C [25]

© 2026 by the author(s). Distributed under a Creative Commons CC BY license.

Preprints.org (www.preprints.org) | NOT PEER-REVIEWED | Posted: 19 March 2026 doi:10.20944/preprints202603.1540.v1

High performance pulsating discharging rate	10-15 C [25]
Gravimetric Energy Density	100–140 Wh/kg [26]
Volumetric Energy Density	220 Wh/L [26]
Thermal Runaway Threshold	180–250 °C [26]
Operation/Storage Range	-30 °C to +60 °C [26]
Typical Lifespan	2,500 to >9,000 cycles [27,28]
Ideal conditions lifespan	10,000 cycles [27,28]

2.3. SoH and RUL Estimation Methods

The health and lifespan of any industrial equipment is very important, the SoH and RUL of all and any industrial equipment is crucial to the maintenance of good operations, from MOSFETs [23], bearings [24,25] and other industrial machinery [26–28]. A battery can be defined specifically as equipment that stores and releases electrical energy. Equipment tends to suffer wear and tear and with time need to be replaced and renewed, in the case of LiBs, degradation is caused by collection of solid electrolyte interfaces (SEI) on the graphite anodes [3,29–33] reducing the amount of lithium ions available in the battery, termed loss of lithium inventory (LLI), causing shorter operating durations at a specific power output. Capacity degradation occurs in two forms called calendar aging and cycle aging, representing loss of capacity when at rest and loss of capacity during usage respectively [33], this paper primarily investigates cycle aging. If the time for this replacement (RUL) is not monitored, a battery or system of batteries may fail to provide the required energy at a critical juncture. More recently, the RUL and SoH of lithium-ion batteries have become matters of scientific research focus because of the growth currently occurring in the clean, green and sustainable energy sectors [16,33–43]. Several methods are used to predict RUL including data driven methods utilizing Neural Networks [31–34], Gaussian processes [35,44], LSTMs [36,38] and physics-based methods have recently been of interest in battery parameter estimation [40,41,44]. Despite these advancements in RUL prediction, model interpretability remains a significant challenge due to the nonlinear, time-variant nature of battery degradation and the strict reliability requirements of critical applications such as electric vehicles and battery energy storage systems. To address this, this paper proposes integrating the Gompertz degradation model with LSTM architecture. This approach aims at enhancing model interpretability by using the Gompertz model not only as a reliable health indicator but also as a mechanism to enforce physics constraints in the network's real-time predictions.

The study evaluates three distinct modelling strategies: (1) a physics-based Gompertz method that models the SoH-RUL relationship as a deterministic decay process (2) purely data-driven Long Short-Term Memory (LSTM) models used to capture temporal dependencies and (3) a hybrid framework called Gompertz-Informed LSTM (GILSTM). By constraining data-driven learning with the Gompertz parameters (k, a and b), the GILSTM approach is designed to combine the predictive power of LSTMs with the interpretability and adherence to physical laws offered by the Gompertz model.

The remaining paper sections are structured as follows: section 3 presents the methodology which includes the rationale for using the Gompertz function, the dataset, dataset analysis and dataset preprocessing; modelling approaches and the modelling rationale, section 4 presents the experimental results, section 5 presents the discussion of comparative evaluation and key limitations, then finally section 6 presents the paper conclusion, key takeaways and suggestions for future work.

3. Materials and Methods

This section outlines the basis for using the Gompertz function, the dataset characteristics and the methodological framework employed in this study. It describes and explores the dataset used, the implementation of pure data-driven models utilizing LSTMs, empirical modelling based on the Gompertz decay function and a novel hybrid approach: Gompertz-Informed LSTM (GILSTM). This hybrid architecture proposes to combine the generalizability of the data-driven techniques with the interpretability and robustness of an empirical modelling approach to accurately estimate Remaining

© 2026 by the author(s). Distributed under a Creative Commons CC BY license.

Preprints.org (www.preprints.org) | NOT PEER-REVIEWED | Posted: 19 March 2026 doi:10.20944/preprints202603.1540.v1

Useful Life (RUL) at specific State of Health (SoH). The overall workflow adopted for this study is visualized in Figure 1 below.

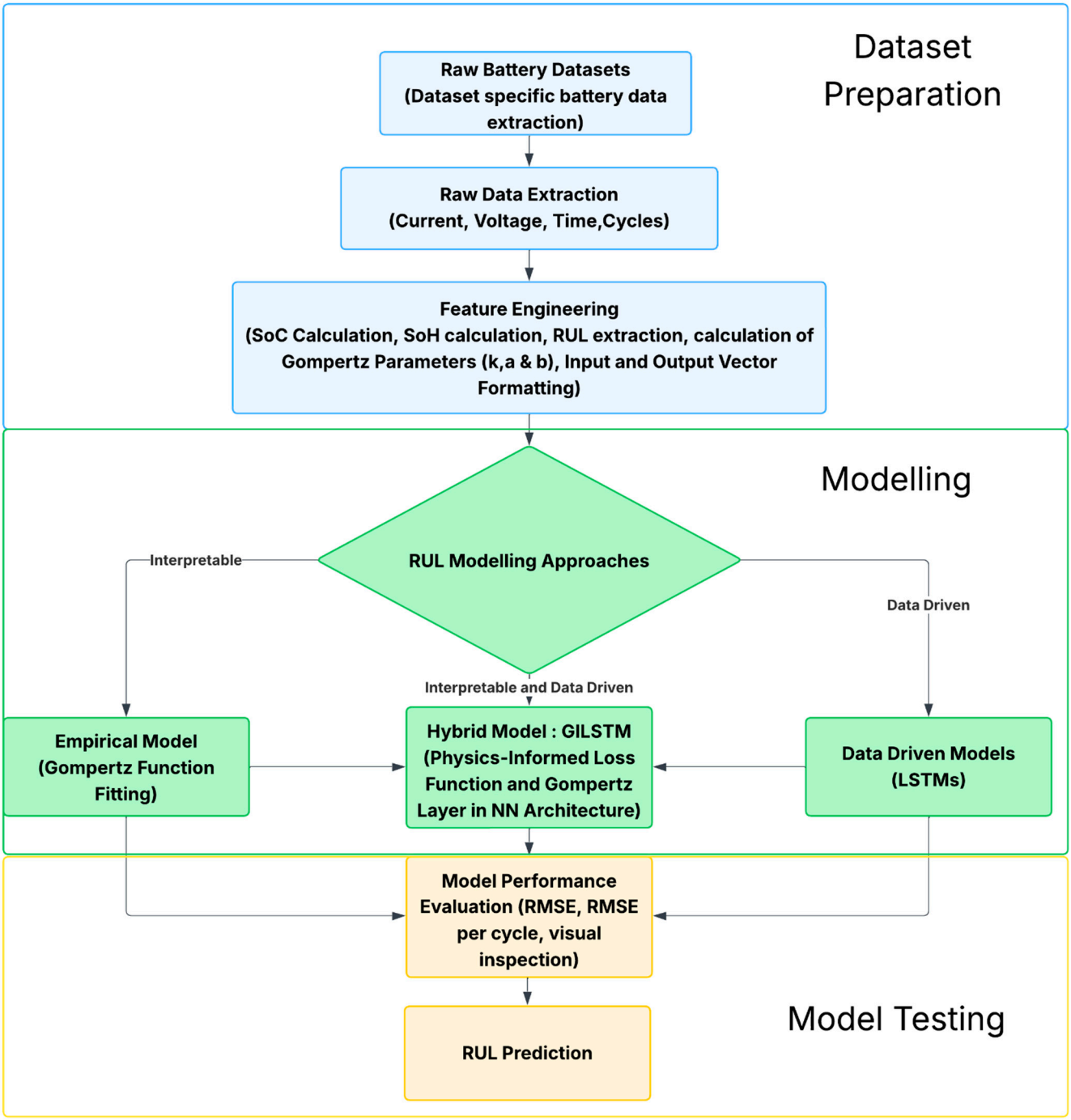

Figure 1. Data and Machine Learning Pipeline.

The key parts of Figure 1 were dataset preparation, modelling and model testing. Dataset preparation involved acquisition of available online LFP battery datasets, conversion of the raw data to pandas data frames where variables such as Current, Voltage, Time and Cycles were extracted from the dataset and using Equation 1 this data was feature engineered to calculate SoC thus, by obtaining the maximum SoC relative to nominal capacity, the SoH of each cell at each cycle was computed. The RUL was extracted for each cell at 70% normalized SoH and the resultant SoH curves were used to compute the Gompertz Parameters (k, a and b) to be used as physical constraints for

© 2026 by the author(s). Distributed under a Creative Commons CC BY license.

Preprints.org (www.preprints.org) | NOT PEER-REVIEWED | Posted: 19 March 2026 doi:10.20944/preprints202603.1540.v1

hybrid models. Modelling involved comparing three distinct approaches to predict RUL. Model testing was the final stage used to evaluate each model's effectiveness.

3.1. Basis for Using Gompertz Parameters for RUL Prediction

3.1.1. Monotonicity and RUL Prediction

LiB capacity degradation is inherently a downward monotonic process. While predicting the SoH at future cycles is a common approach to estimating the RUL, direct multistep forecasting often suffers from error accumulation (drift) as the prediction horizon increases. To address this contention around predicting RUL, this study proposes an inverse mapping strategy. Rather than predicting the SoH for a given cycle, the model predicts the number of cycles required to reach 0.7 SoH threshold. Thus, RUL prediction is reformulated as determining the number of cycles the battery in its current state will take to reach its End of Life (EoL) threshold. This approach leverages the monotonic nature of capacity degradation, mapping observed data to a specific destination (the RUL at EoL). As illustrated in Figure 2, the proposed method predicts the point of failure by estimating the number of cycles required to reach a SoH of 0.7, enforcing a strictly monotonic decay consistent with physical capacity degradation.

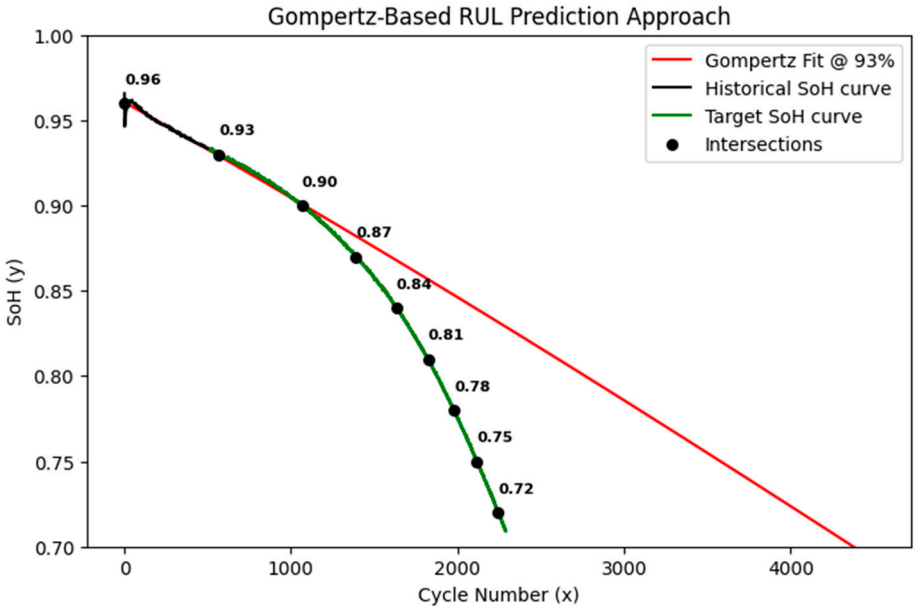

Figure 2. Schematic of the proposed inverse-mapping prediction.

Unlike traditional methods that forecast SoH from cycles or predict RUL, this paper's approach uses an LSTM to predict the k, a and b (Gompertz parameters) and use the inverse Gompertz equation to calculate the corresponding RUL from the x-axis. The Gompertz model can on its own be used to predict close SoH intervals, for example, in Figure 2 the Gompertz fit for SoH data from Beginning-of-Life (BoL) to 93% SoH (511 cycles of historical data) can be used to calculate the cycles needed to reach 0.9 SoH but can an LSTM trained using constraints informed by the Gompertz model accurately predict the k, a and b parameters that would calculate the RUL accurately? The Gompertz fit at 93% SoH approximates a RUL of 4452 cycles. The theoretical Gompertz degradation path (red curve) serves as a physics-informed constraint, guiding the LSTM's k, a and b values to predict the SoH curve (green line) while ensuring monotonic degradation behaviour. By predicting the RUL, the model combines the data-driven benefits of neural networks with physics informed constraints derived from the Gompertz growth model [45].

3.1.2. The Gompertz Model

© 2026 by the author(s). Distributed under a Creative Commons CC BY license.

Preprints.org (www.preprints.org) | NOT PEER-REVIEWED | Posted: 19 March 2026 doi:10.20944/preprints202603.1540.v1

The Gompertz model [45] is a widely established sigmoidal function commonly used to describe growth and degradation processes, owing to its asymptotic behaviour, interpretability and ability to model nonlinear trends such as growth and degradation phenomena. In this study, the Gompertz function is used to approximate the capacity degradation curve of LFP batteries and estimate their RUL. The general form of the Gompertz function [45] is defined in Equation 3a.

$$y(x) = ke^{-e^{a-bx}} \tag{3a}$$

where

- $y(x)$ denotes the normalized capacity at cycle x.
- k is a scaling factor representing initial capacity.
- a is a shape parameter controlling the shift of the curve.
- b controls the rate of capacity degradation.

The model parameters (k, a, b) are estimated using non-linear least squares optimization. Equation 3a can be rearranged to Equation 3b to solve for x (cycles) given a specific target SoH ($\hat{y}$), facilitating the inverse mapping strategy described in Section 3.1.1.

$$x = \frac{a - \ln\left(\ln\left(\frac{k}{y}\right)\right)}{b} \tag{3b}$$

Furthermore, to ensure the neural network adheres to physical degradation laws, the differential form of the Gompertz equation is utilized as a constraint during training. This enforces a Physics-Informed framework where the network outputs satisfy the rate of change defined by Equation 3c.

$$\frac{dy}{dx} = bye^{a-bx} \tag{3c}$$

By integrating Equation 3c into the loss function, the model is constrained to obey the mathematical properties of the Gompertz degradation trend, ensuring robust and interpretable RUL predictions.

3.2. Dataset Acquisition and Description

The dataset used for experimentation and pipeline development in this study was the Huazhong University of Science and Technology (HUST) battery dataset [36]. The HUST battery dataset was downloaded directly from Mendeley data. The raw HUST dataset comprises of charging and discharging data from 77 LFP cells, each with a nominal capacity of 1.1 Ah. From the data, all cells were cycled using a standardized charging protocol, with different multistage discharge protocols applied to the cells at a constant temperature of 30 °C to ensure thermal consistency across the dataset. The dataset is meant to be used to model battery health, thus relevant to the study in this paper. The raw HUST data has been packaged in pickle format (.pkl) and are serialized python objects that had been converted into a byte stream for storage purposes.

3.3. Dataset Analysis and Preparation

The raw HUST data was stored in dictionary format, that dictionary contained three nested dictionaries, the first contained data representing the calculated RUL at each battery cycle, the second contained the battery capacity after each cycle and the third contained data indicating the charging status, cycle number, current in milliamperes, voltage, capacity of stored power and the time since the cycle started. To conduct the study in this paper, the data was aggregated into a refined dataset. The refined dataset includes six dependent variables: current, voltage, cell capacity (Q), RUL, cycle number, and change in capacity (dq) as well as two independent variables: time and cycle count. Figure 3 shows how these variables change over time for cell 2-2. The plots are of the dependent variables over time for all cycles of cell 2-2 from the HUST dataset on the left (a) and on the right (b) are the same plots over time but only for the first ten cycles.

© 2026 by the author(s). Distributed under a Creative Commons CC BY license.

Preprints.org (www.preprints.org) | NOT PEER-REVIEWED | Posted: 19 March 2026 doi:10.20944/preprints202603.1540.v1

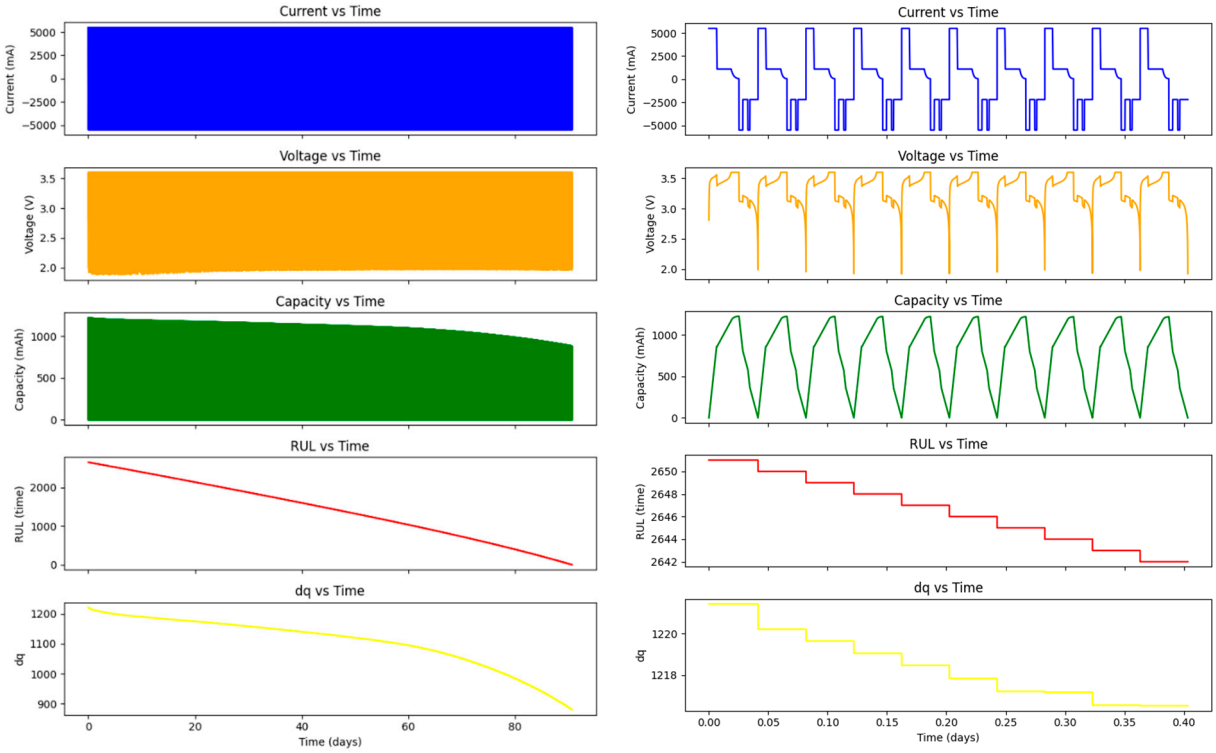

Figure 3. The plots of the dependent variables over time for cycles of cell 2-2.

The RUL of the cell equalled zero when the usable cell capacity dropped to 880 mAh (80% of the nominal capacity). Figure 3 (b) zooms in to the first ten cycles (9.7 hours) of Figure 3(a), showing how the dependent variables evolved with each charge-discharge cycle within those 10 cycles, while Figure 3 (a) shows how those dependent variables evolved over the entire lifespan of the battery (2651 cycles/90 days). The HUST dataset had data from variables of voltage, current, time, capacity, dq and cycles to model SoH and RUL, it was required to understand the relationship between these variables and how they can be used to obtain SoC and SoH. For the SoC to be computed, the Coulomb Counting SoC estimation formula shown in Equation 1 was used because SoH is defined as the ratio of the capacity of a battery in a used state and a new state [46–48], moreover since the Coulomb Counting SoC equation uses the rated capacity instead of the current capacity, this detail is reinforced. As mentioned earlier the coulomb counting equation typically uses the nominal capacity to calculate SoC, if a SoH degradation model such as an LSTM or a Gompertz model is used, the capacity can be adjusted such that each percentage value of the SoC from 0% to 100% of each cycle is corrected, that is, 1% should represent 1% of the current capacity not rated capacity, for early, mid and later cycles. The SoH formula is represented as in Equation 4, where $C_{current}$ stands for the cell capacity at time t and C_{rated} is the nominal capacity of the cell.

$$SoH(t) = \frac{C_{current}}{C_{rated}} = \frac{\max(SoC)}{C_{rated}} \quad (4)$$

Since the HUST cells were charged and discharged to more than the nominal capacity of 1.1Ah, each cell was normalized by 115% of 1.1Ah to ensure they are bound between 0 and 1. This is attributed to the conservative manufacturer ratings and the capacity buffer typically found in new cells [49,50]. By using a normalization factor of 1.265Ah (115% of nominal capacity), the SoH normalization in Equation 5 accounts for the or the fact that new high-quality cells often exhibit an initial capacity significantly higher than their labelled nominal capacity. This ensures that the normalized SoH do not exceed 1.0 at the Beginning of Life (BoL) which would otherwise distort the

© 2026 by the author(s). Distributed under a Creative Commons CC BY license.

Preprints.org (www.preprints.org) | NOT PEER-REVIEWED | Posted: 19 March 2026 doi:10.20944/preprints202603.1540.v1

training of machine learning models like LSTM; thus the 80% of the nominal capacity is normalized to 70% SoH.

$$normalized\ SoH(t) = \frac{SoH}{115.0} \quad (5)$$

Following the completion of data preprocessing and calculations, the capacity values for e ach cycle were extracted, enabling subsequent analysis of degradation trends. For training, validation and testing purposes, the dataset was split with the ratio 72:14:14, resulting in 55 cells for training, 11 cells for validation and 11 cells for testing, the exact splits were based on BatteryML's [44] train-test splits, this was to ensure consistency when comparing results. In Figure 4, the SoH values obtained from the SoH normalization formula Equation 4 are used and the cycle number has been normalized by 10,000 cycles, the expected upper limit number of cycles. The batteries in the HUST dataset used more than the nominal capacity of 1.1 Ah with many reaching 1.21 Ah. To ensure uniformity among all the datasets, 1.265 Ah was used as the normalizing constant for all datasets used as shown in Equation 5.

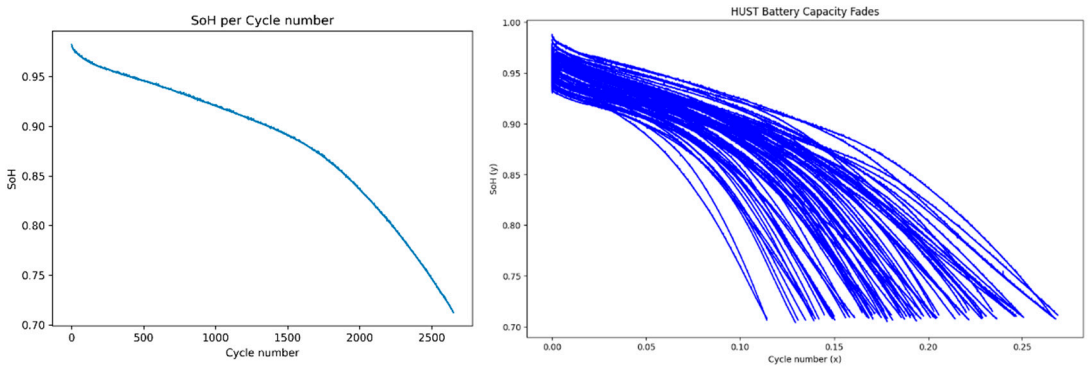

Figure 4. The plot of normalized SoH versus cycle number for cell 2-2 (left) and a plot of SoH versus normalized cycle count is plotted for all 77 HUST cells.

3.4. Modelling

3.4.1. Gompertz Model Formulation

The Gompertz model is a growth model developed by Benjamin Gompertz in 1825 to model human mortality [45]. The Gompertz model was utilized in two experiments, the first set of experiments fit the model on entire SoH curves like those shown in Figure 4, thus extracting their final k, a and b, then finally calculating the RUL using Equation 3b where y = 0.7 and checking the Gompertz model's ideal performance. This method is referred to as the baseline Gompertz fit. The second method was testing the Gompertz model real time RUL estimation performance from cycle 1 to cycle N where N ranged from value 2 to value 2689 (the longest cell lifespan of any of the HUST cells). For the second method, the inverse Gompertz equation (Equation 3b) was also used. This method is referred to as Real-Time Gompertz Testing. Data analysis was conducted to explore the relationship between the Gompertz parameters k, a and b and the battery RULs.

A. Baseline Gompertz Fit

In an ideal situation, the entire SoH curve of each battery is known by some form of successful extrapolation thus fitting the Gompertz function to these curves results in values of k, a and b whose calculated RULs should have very little deviation from the target RULs. By doing this, the study shows the potential performance of the Gompertz model. Figure 5 shows the pipeline used to calculate the RUL using the Gompertz function.

© 2026 by the author(s). Distributed under a Creative Commons CC BY license.

Preprints.org (www.preprints.org) | NOT PEER-REVIEWED | Posted: 19 March 2026 doi:10.20944/preprints202603.1540.v1

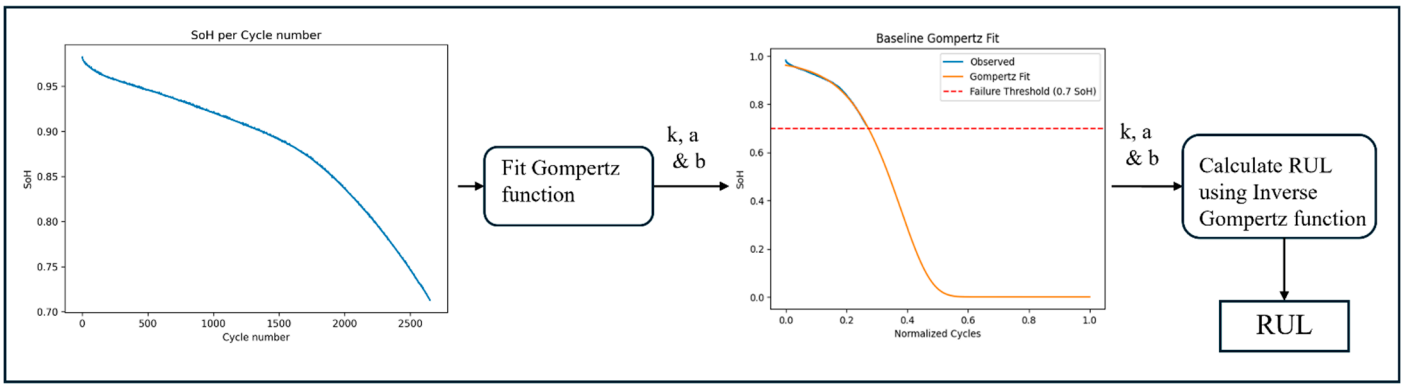

Figure 5. Schematic of the RUL estimation framework using the Gompertz function.

The observed SoH on the left was fitted to the model to extract parameters k, a and b, these parameters are used as targets in the GILSTM later. The parameters were used to calculate the exact point of intersection with the failure threshold by using the Inverse Gompertz function, Equation 3b, where y = 0.7, resulting in predicted RUL values.

B. Real-Time Gompertz Testing

In practice, the complete SoH curves are not known if the cell has not reached its RUL, the curves need to be approximated from the known values of SoH. Each cell would have SoH values ranging from cycle 1 to cycle N where N ranged from value 2 to value 2689 (the longest cell lifespan of any of the HUST cells), interval of 1 cycle. The schematic pipeline for this is shown in Figure 6. As illustrated in Figure 6, the parameters k, a and b are subsequently used in Equation 3b to estimate the RUL by extrapolating the cycle x at which the SoH drops to 0.7 due to normalization in Equation 5 the SoH values of 110% to 80% are represented within the range 0.96 to 0.7.

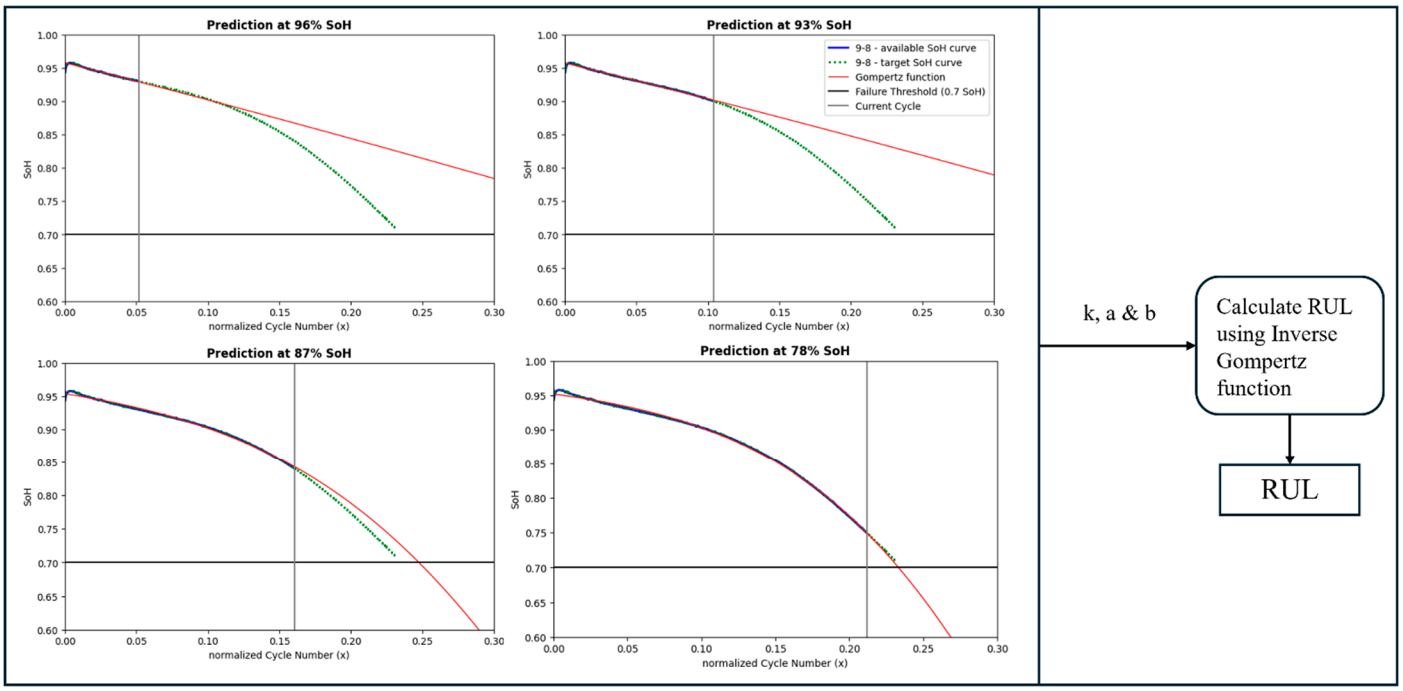

Figure 6. Schematic of the Realtime-fitting procedure.

Figure 6 above describes how the Gompertz model fits on available data and how RUL is calculated at different cycle numbers and SoH thresholds. The Gompertz model was fitted on truncated SoH curves representing different stages of battery life (96%, 93%, 87%, and 78% SoH). The vertical gray line indicates the current cycle available for fitting; the red curve shows the Gompertz

© 2026 by the author(s). Distributed under a Creative Commons CC BY license.

Preprints.org (www.preprints.org) | NOT PEER-REVIEWED | Posted: 19 March 2026 doi:10.20944/preprints202603.1540.v1

model's extrapolation used to calculate RUL at that specific cycle. The main limitation was how to capture long temporal dependencies, especially given how the SoH curve has a non-linear shape. When calculating the RUL, the values were multiplied by 10,000 to obtain the non-normalized RUL values.

3.4.2. Long Short-Term Memory (LSTM) Models

LSTM networks [51] are a type of recurrent neural network (RNN) capable of learning long-term dependencies in sequential data. Due to their memory nodes, LSTMs are particularly effective at modelling time series data with temporal correlations, such as battery capacity degradation patterns across multiple charge-discharge cycles. In this study, two LSTMs were developed to model SoH to RUL using two separate strategies and the same models were used as the backbone neural network in the GILSTMs section 3.4.3. The two models can be classified in this manner:

A. An LSTM that directly predicted RUL from SoH values (LSTM1).
B. An LSTM-based that predicted the next cycle's SoH from SoH values (LSTM2).

These models were used as baseline Blackbox models. For each of these models, the same backbone LSTM predictor was used with the main differences being the mentioned outputs, the training strategy as well as testing strategies. The architecture of each of these models is shown in Figure 7. Both models take a sequence of normalized SoH values as input, these values are derived from the SoC calculations over a fixed window of prior cycles, here a window size of 100 cycles is used. LSTM1 outputs a single RUL prediction. LSTM2 outputs the next cycle's SoH value, the RUL is obtained from it by recursively popping out the first value in the window, shifting the remaining window forward by one and popping in the predicted SoH value at the end of the window then running the model on this new window. The number of cycles needed to output a SoH prediction lower than 80% of the nominal capacity is taken as the predicted RUL. This type of LSTM is known as a sequence-to-one LSTM.

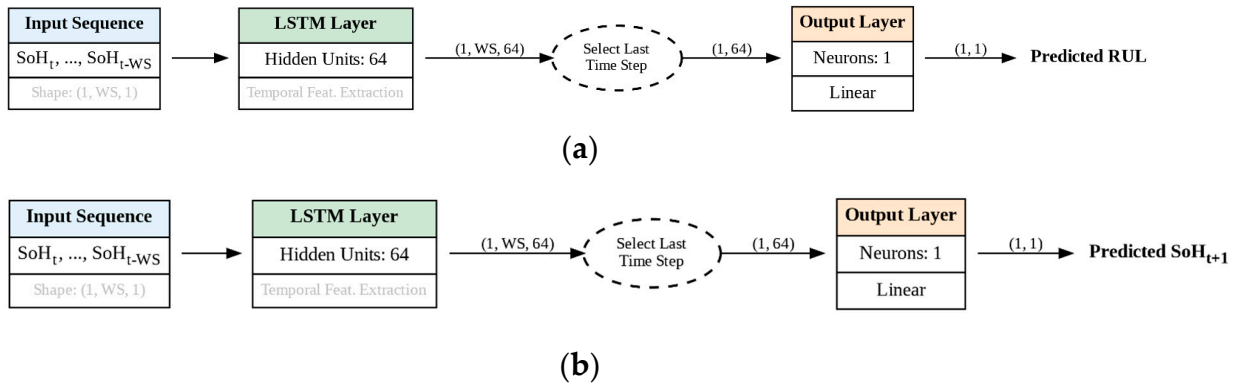

Figure 7. (a). The labelled architecture for the SoH to RUL LSTM (LSTM1). **(b).** The labelled architecture for the SoH-to-SoH LSTM (LSTM2).

These two models are baseline data driven LSTM models for comparison with the GILSTMs. The approaches leverage the LSTM's ability to capture non-linear and temporal dynamics in battery behaviour enabling accurate RUL estimation. Since these two models were formulated as similar sequence-to-one regression tasks as seen in Figure 7, their input tensors are similar and of shape [batch_size, window_size, 1], where window_size refers to the number of time steps used in each prediction. Experiments were conducted with a window size of 100.

Training Setup

Model training and inference were conducted on a POSIX-compliant Linux x86_64 system with a P100 GPU and on a POSIX-compliant Linux x86_64 system with 4 NVIDIA GH200 GPUs. The networks were trained using the Adam optimizer [52] with an initial learning rate of 1e-3. To improve convergence, a StepLR learning rate scheduler was employed with a step size of 200 epochs. The

© 2026 by the author(s). Distributed under a Creative Commons CC BY license.

Preprints.org (www.preprints.org) | NOT PEER-REVIEWED | Posted: 19 March 2026 doi:10.20944/preprints202603.1540.v1

Mean Squared Error (MSE) was used as the loss function, and performance was evaluated using Root Mean Squared Error (RMSE) on both training and validation datasets. The models with the best validation loss were saved. The number of training epochs set at 1000 as shown in Table 3 was determined empirically by monitoring the validation RMSE. Training continued for all 1000 epochs but only the best model was saved.

Table 3. Key Training hyperparameters.

Loss Function	Mean Squared Error (MSE)
Learning Rate Scheduler	StepLR (step size = 200)
Optimizer	Adam(lr=1e-3)
Epochs	1000
Evaluation Metric	Root Mean Squared Error (RMSE)

3.4.3. Gompertz-Informed Long Short-Term Memory (GILSTM) Models

In this study there were three GILSTM models developed to leverage the advantages of LSTMs and the Gompertz function to model battery capacity degradation. The three models were classified as follows:

A. A GILSTM that directly predicted the parameters k, a and b from SoH values (GILSTM1) trained only on SoH data from the first 100 cycles only. For the inference stages, the predicted k, a and b were passed through an inverse Gompertz layer to predict each test cell's RUL.
B. A GILSTM that directly predicted the parameters k, a and b from SoH values (GILSTM2) trained on SoH data from all cycles. For the inference stage, the predicted k, a and b were passed through the inverse Gompertz layer to predict each test cell's RUL. This inverse Gompertz layer is based on the Equation 3b.
C. A GILSTM that predicts RUL using LSTM2, the model predicts the next cycle's SoH from SoH values (GILSTM3), when used recursively can predict the RUL. The Gompertz function was fitted on the recursively output SoH curve and using the generated k, a and b parameters were passed through the inverse Gompertz layer to predict each test cell's RUL.

GILSTM1 and GILSTM2 both utilize the architectures described in Figure 8. The architectures are different depending on whether the model was training, Figure 8 (a) or inferencing, Figure 8 (b). When inferencing the inverse Gompertz function was used to calculate RUL.

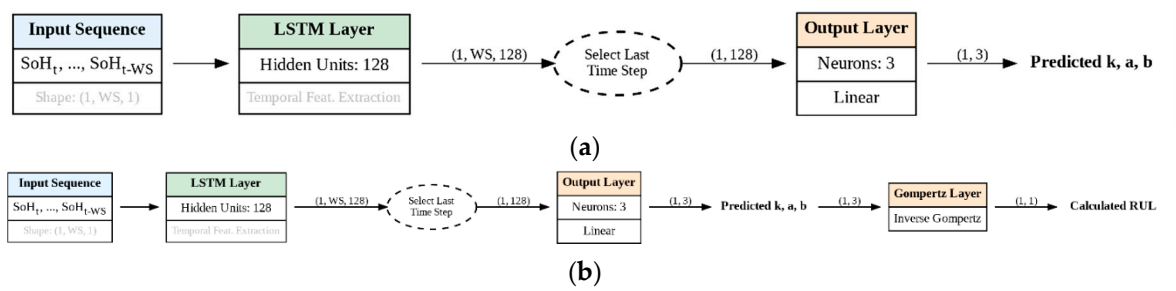

Figure 8. (a). The architecture for GILSTM1 and GILSTM2 used in training. **(b).** The architecture for GILSTM1 and GILSTM2 used during inference.

The purpose of these models, GILSTM1 and GILSTM2, having to predict the parameters first was to ensure the models learnt the physical degradation of the battery's capacities. Training of these models utilized the same hardware used to train and test the purely data-driven models. The training process of these Gray-Box models is shown in Figure 9 and utilizes a weighted loss comprising of data loss, physics loss and RUL loss to guide the training process. The Physics-Informed Loss function is described in more detail in Figure 10. The overall weighted function used in training combines the data loss, the MSE between the target k, a and b and the predicted k, a and b, the physics loss, MSE

© 2026 by the author(s). Distributed under a Creative Commons CC BY license.

Preprints.org (www.preprints.org) | NOT PEER-REVIEWED | Posted: 19 March 2026 doi:10.20944/preprints202603.1540.v1

between the target and predicted 1st derivative of the Gompertz function ($\frac{dy}{dx}$) and the MSE between the target and predicted Gompertz function (y) and an RUL loss where the predicted k, a and b were passed through an inverse Gompertz layer where y was 0.7, calculating the predicted RUL and then calculating the MSE between predicted RUL and target RUL. The GILSTM3 model leveraged the superior learning of the LSTM network to capture the underlying capacity fading shape and the Gompertz function used the capacity fade curve output from the LSTM to fit the parameters k, a and b of a Gompertz degradation function. RUL prediction from these fitted k, a and b is then conducted.

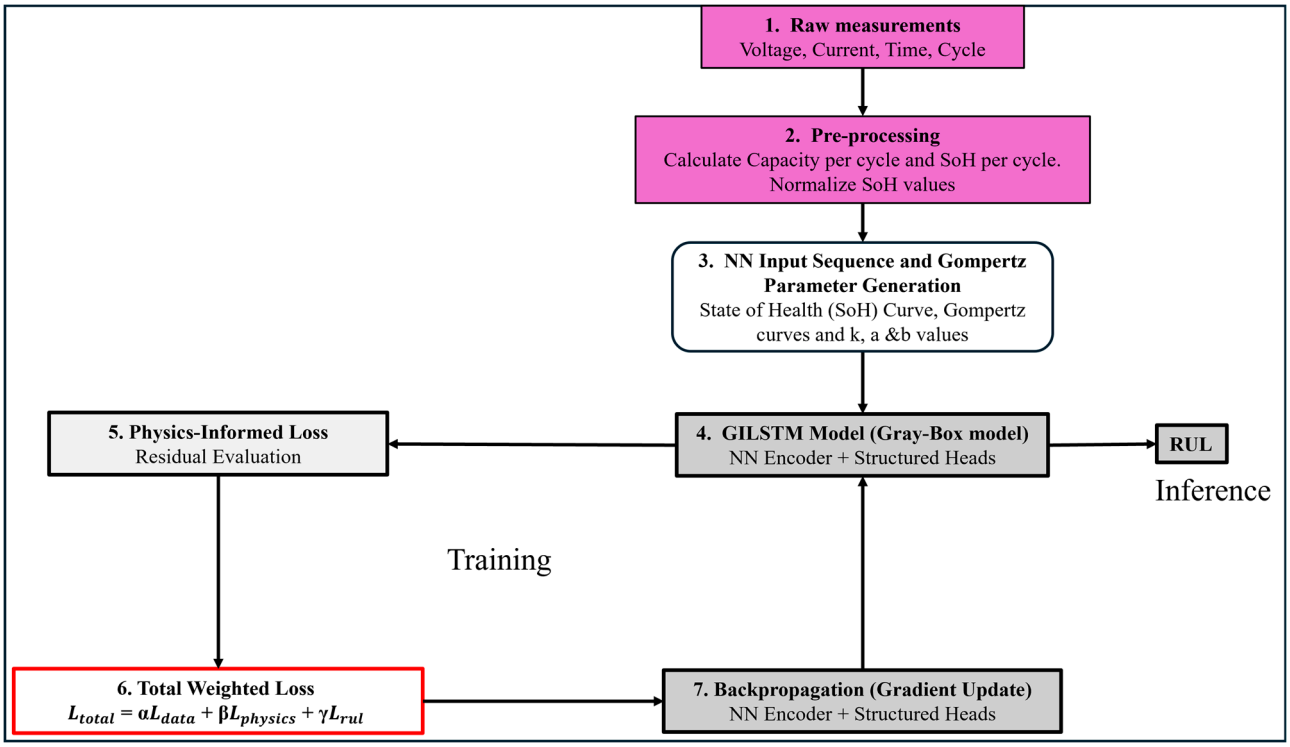

Figure 9. The training process for GILSTM1 and GILSTM2.

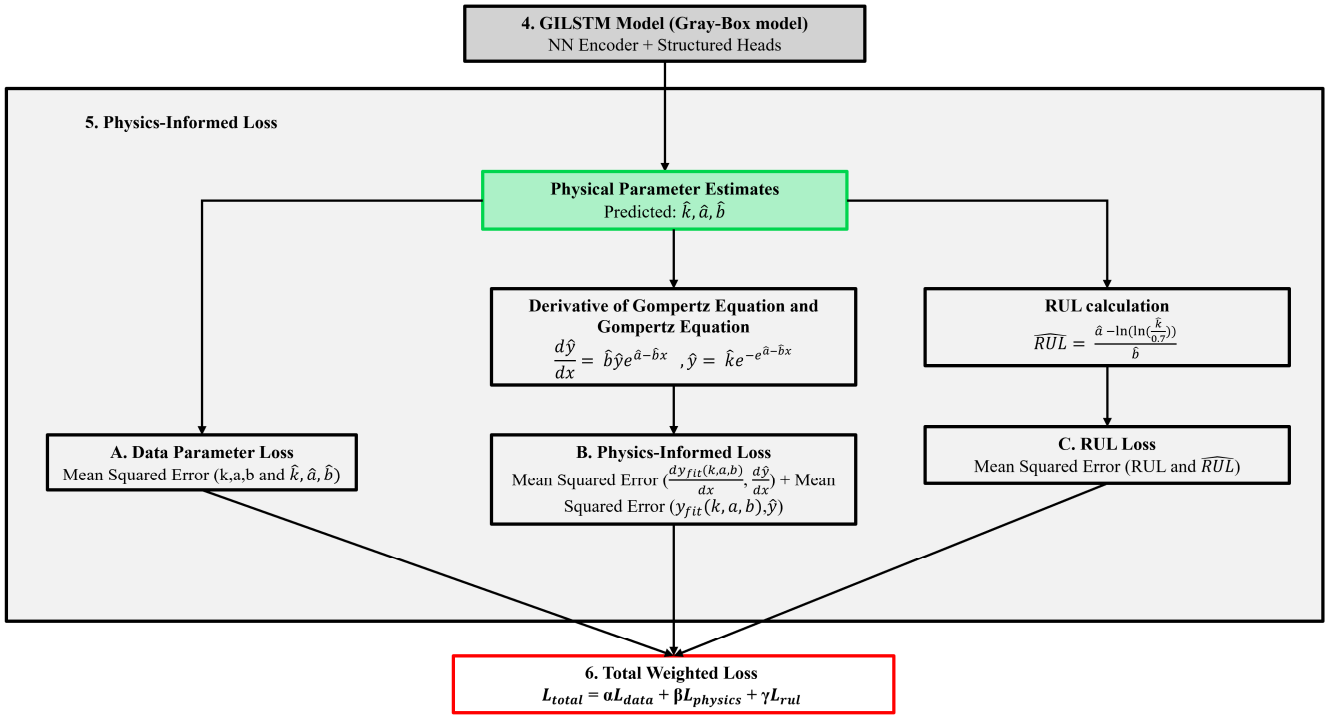

Figure 10. The Physics-Informed Loss used for training GILSTM1 and GILSTM2.

© 2026 by the author(s). Distributed under a Creative Commons CC BY license.

Preprints.org (www.preprints.org) | NOT PEER-REVIEWED | Posted: 19 March 2026 doi:10.20944/preprints202603.1540.v1

3.5. Evaluation Metrics

Five evaluation methods were utilized to evaluate quantitatively the performance of the proposed models: mean squared error (MSE), physics-informed loss function, root mean squared error (RMSE), RMSE per Cycle and RMSE at cycle 100.

a. Mean Squared Error (MSE) - measures the average of the squares of the error [43].

$$MSE = \frac{1}{n}\sum_{i=1}^{n}(y_i - \hat{y}_i)^2 \quad (6)$$

The MSE is sensitive to outliers and used in regression models. Used when training all models, when training GILSTM1 and GILSTM2 the MSE was used to formulate the physics-informed loss function as shown in Figure 10.

b. Physics-Informed Loss Function

To train GILSTM1 and GILSTM2 it was seen fit to penalize the model for disobeying downward monotonicity since the Gompertz function captures that trend from the SoH curves, to achieve that the MSE in the first derivative $\frac{dy}{dx}$, in the Gompertz Function, the RUL as well as the Gompertz parameters k, a and b were used as shown in Figure 9 and in the weighted loss function shown in Figure 10. Use of the first derivative was influenced by the PINNs paper [53] as well as the fact that the first derivative had a very high correlation with the cell's RUL. This resulted in a weighted loss comprising of data loss, physics loss and RUL loss to guide the training process.

c. Root Mean Squared Error (RMSE) - Square root of MSE. Sensitive to outliers and is in the same unit as the original data. %RMSE is the RMSE divided by the mean target RUL.

$$RMSE = \sqrt{\frac{1}{n}\sum_{i=1}^{n}(y_i - \hat{y}_i)^2} \quad (7)$$

d. RMSE vs Cycle

Used to evaluate how the models RUL RMSE changes as batteries degrade across their cycle life. Confirms model generalizability over time.

e. RMSE at cycle 100

Used as a benchmark result particularly because of work from Severson et. al [35] and BatteryML [44]. Since predicting RUL is harder in early stages, this benchmark is a realistic way of comparing the performance of different models on RUL prediction. This benchmark relies on testing the model on data from the first 100 cycles only.

4. Results

This section outlines the results from Gompertz data analysis, visualized and numerical results from the modelling processes, particularly the results of empirical modelling based on the Gompertz decay function, pure data-driven models utilizing LSTMs (LSTM1 and LSTM2) and novel hybrid approaches: Gompertz-Informed LSTM (GILSTM1, GILSTM2 and GILSTM3).

4.1. Gompertz Data Analysis and Modelling Results

The initial experimentation with the Gompertz function was to provide baseline and real-time results when using the Gompertz model for RUL prediction.

4.1.1. Gompertz Parameter Data Analysis and Baseline Gompertz Fit

This section sought to establish justifiable reasons as to why the Gompertz model is suitable for making LSTMs and neural networks more interpretable when predicting RUL. The results of these experiments are on full SoH curves. Thus, prior to development of RUL prediction models, the relationships between SoH and the Gompertz parameters and between RUL and the Gompertz parameters were investigated. This initial experimentation was to check whether the Gompertz model had captured any valuable information that was relevant to the cells' RUL. The variables represented the values captured from the cell's full SoH curves. It was found that the values for the Gompertz parameters

© 2026 by the author(s). Distributed under a Creative Commons CC BY license.

Preprints.org (www.preprints.org) | NOT PEER-REVIEWED | Posted: 19 March 2026 doi:10.20944/preprints202603.1540.v1

k, a and b shown in Figures 11 (a), (b) and (c) respectively ranged between 0.93 to 1.2 for k, -4.6 to -1.5 for a and -28 to -4 for b. The parameter b shows a strong positive correlation with RUL. This reinforces the thought that the Gompertz function may be useful when predicting battery RUL.

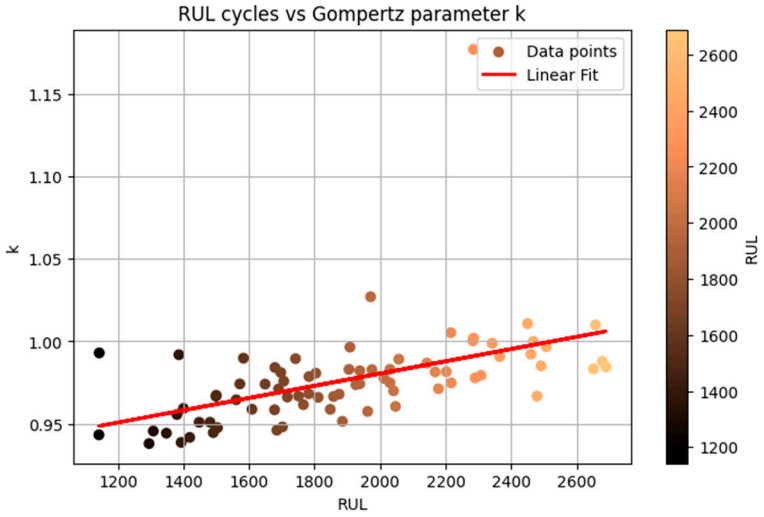

(a)

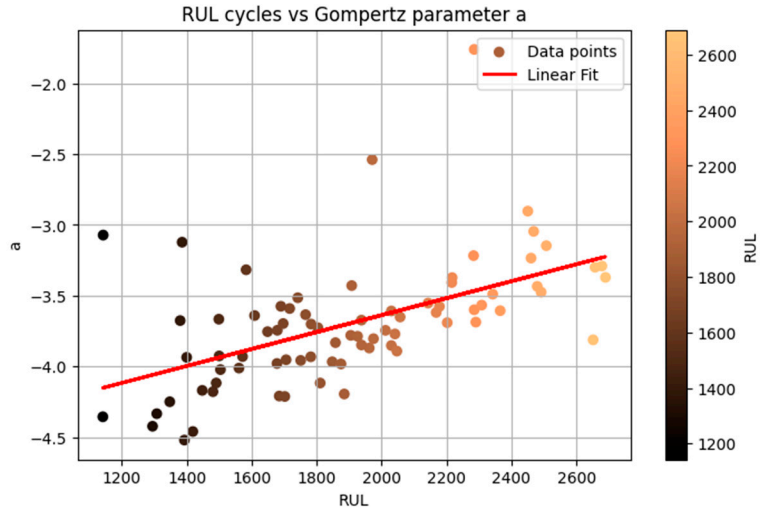

(b)

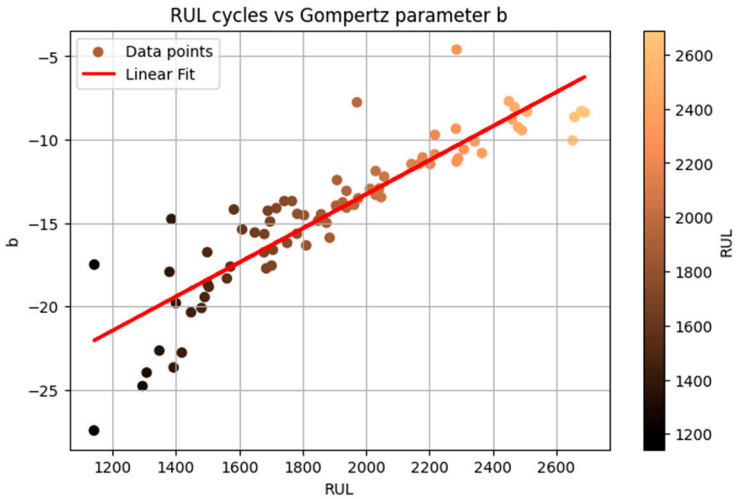

(c)

© 2026 by the author(s). Distributed under a Creative Commons CC BY license.

Preprints.org (www.preprints.org) | NOT PEER-REVIEWED | Posted: 19 March 2026 doi:10.20944/preprints202603.1540.v1

Figure 11. a, b and c represent the linear relationship between the Gompertz Parameters k, a and b respectively with RUL.

Moreover, Figure 11 confirms correlations for parameters k, a and b with RUL seen in the correlation matrix in Figure 12 where parameter b has the highest correlation of 0.89 followed by parameter a and parameter k.

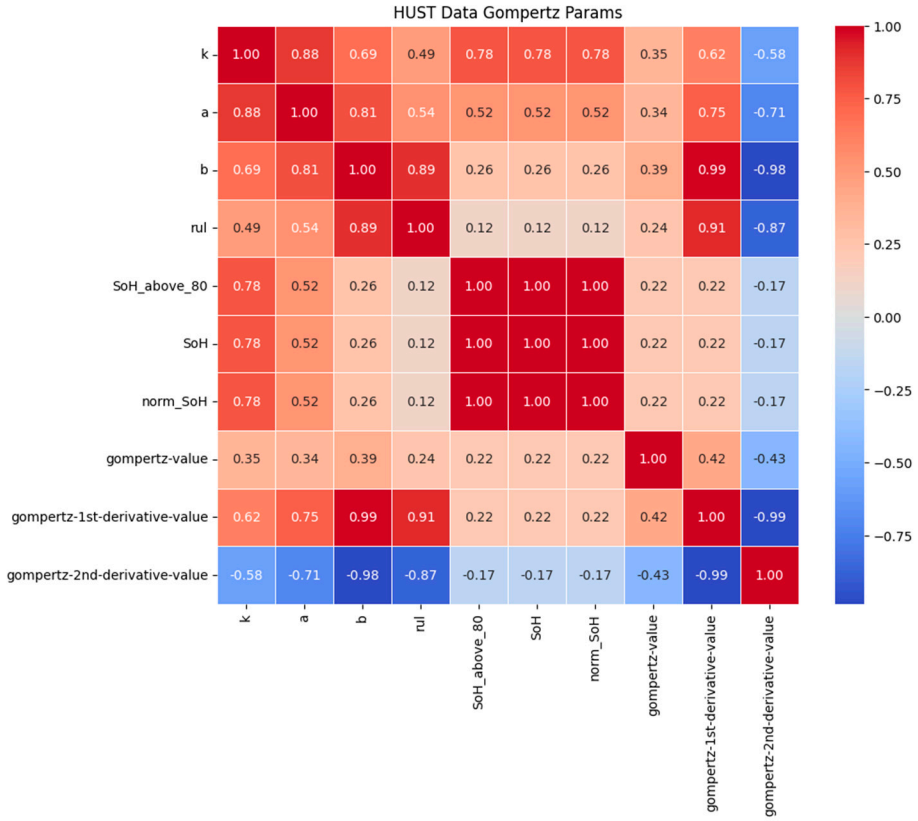

Figure 12. The correlations between HUST data and Gompertz parameters.

In Figure 12, what is particularly important is the high correlation between parameter b, the 1st derivative of the Gompertz equation and RUL. This high correlation informed the use of the first derivative in the physics-informed loss. The various tranches of RUL were 14 cells that had a RUL of 1000 – 1500, 34 cells with a RUL of 1500-2000 and 29 cells with a RUL of more than 2000. As part of the study the relationship between these three various tranches of RUL and the Gompertz parameters k, a and b were investigated and shown in Figure 13. The variable b delineates these tranches quite well.

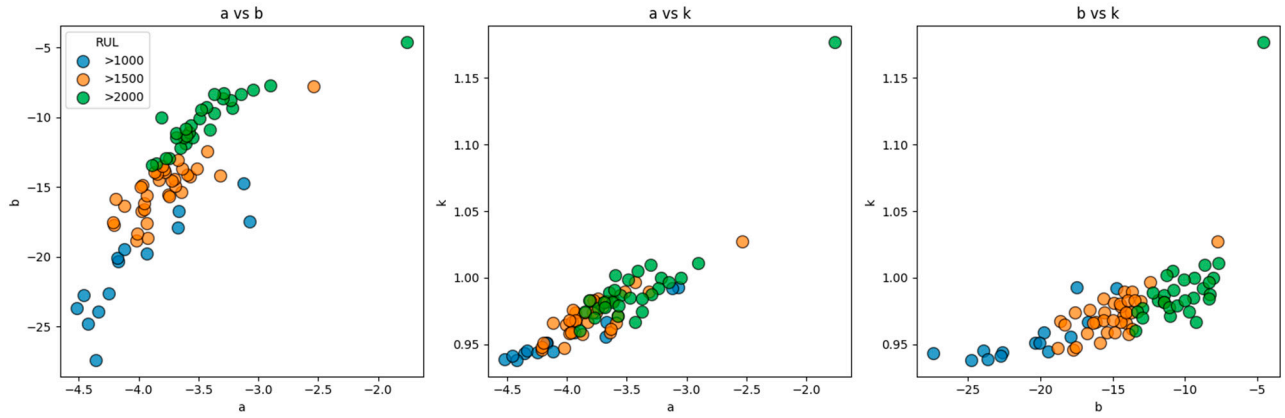

© 2026 by the author(s). Distributed under a Creative Commons CC BY license.

Preprints.org (www.preprints.org) | NOT PEER-REVIEWED | Posted: 19 March 2026 doi:10.20944/preprints202603.1540.v1

Figure 13. The relationship between a and b (left), a and k (middle) and b and k (right) colour-coded according to those RUL categories.

Figure 13 proves that the Gompertz function can be used to confirm the RUL of a cell given complete SoH curves. Furthermore, the cells' complete SoH curves were fitted on the Gompertz function, and the RUL was calculated using the inverse Gompertz function Equation 3b resulting in a mean RMSE of 27.9 cycles (1.4%). Such results would be excellent, but they can only be calculated given the actual SoH curves are known.

4.1.2. Modelling Results

Below is Table 4 representing the results of the various models developed in this study as well as the results of comparable studies. The units of RMSE are in cycles.

Table 4. Modelling results.

Model	100th Cycle RMSE (%RMSE)	Mean RMSE (mean %RMSE) per cycle
Baseline Gompertz	Not Applicable	27.9 (1.4%)
Real-Time Gompertz	16250 (861.89%)	3192 (167.6%)
SoH-RUL LSTM (LSTM1)	321 (17.02%)	188 (9.87%)
SoH-SoH LSTM (LSTM2)	327 (17.34%)	182 (9.18%)
SoH-k,a,b GILSTM (GILSTM1)	408 (21.64%)	657 (29.54%)
SoH-k,a,b GILSTM (GILSTM2)	431 (22.86%)	501 (22.97%)
SoH-SoH GILSTM (GILSTM3)	339 (17.98%)	594 (26.99%)
HUST Model [34]	Not Applicable	186 (9.38%)
BatteryML "Discharge" Model (best) on HUST dataset [44]	322 (17.08%)	Not Applicable
BatteryML LSTM Model on HUST dataset [44]	443 (23.5%)	Not Applicable
BatteryML Transformer Model on HUST dataset [44]	391 (20.74%)	Not Applicable
BatLiNet Model on HUST dataset [54]	264 (14%)	Not Applicable

In Table 4, there is presented the performance of the developed models compared to the various baseline models. The baseline "Discharge" model used linear regression on capacity-voltage curves [54] whereas the BatLiNet model uses an Encoder-Decoder neural network with embedding spaces to achieve superior performance. The models developed in this study were also tested on RMSE per cycle resulting in Figure 14.

The relationship between SoH and Gompertz (y), its first and second derivatives, was also investigated for all cells and is shown in Appendix A. The performance failures of the Gompertz function in the early cycles (before cycle 500) can be attributed to the large derivative values exhibited by the Gompertz and shown in Appendix A. As seen in Table 4 and Figure 14, LSTM1 and LSTM2 had the best performance.

The various capacity forecasts were also visually inspected to ensure they were what was expected. Figure 15 below represents some of the test cells with their target SoH and their predicted SoH, these are the curves predicted by LSTM2 since the other models predict direct values instead.

© 2026 by the author(s). Distributed under a Creative Commons CC BY license.

Preprints.org (www.preprints.org) | NOT PEER-REVIEWED | Posted: 19 March 2026 doi:10.20944/preprints202603.1540.v1

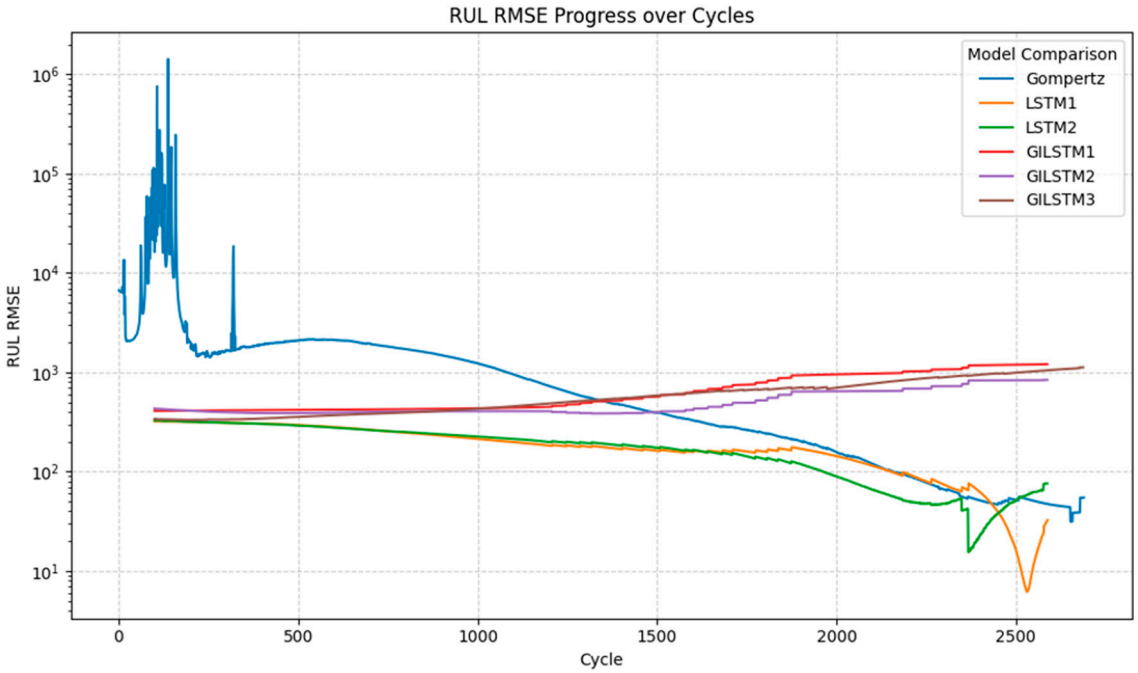

Figure 14. The RMSE per cycle for each of the models developed in this study.

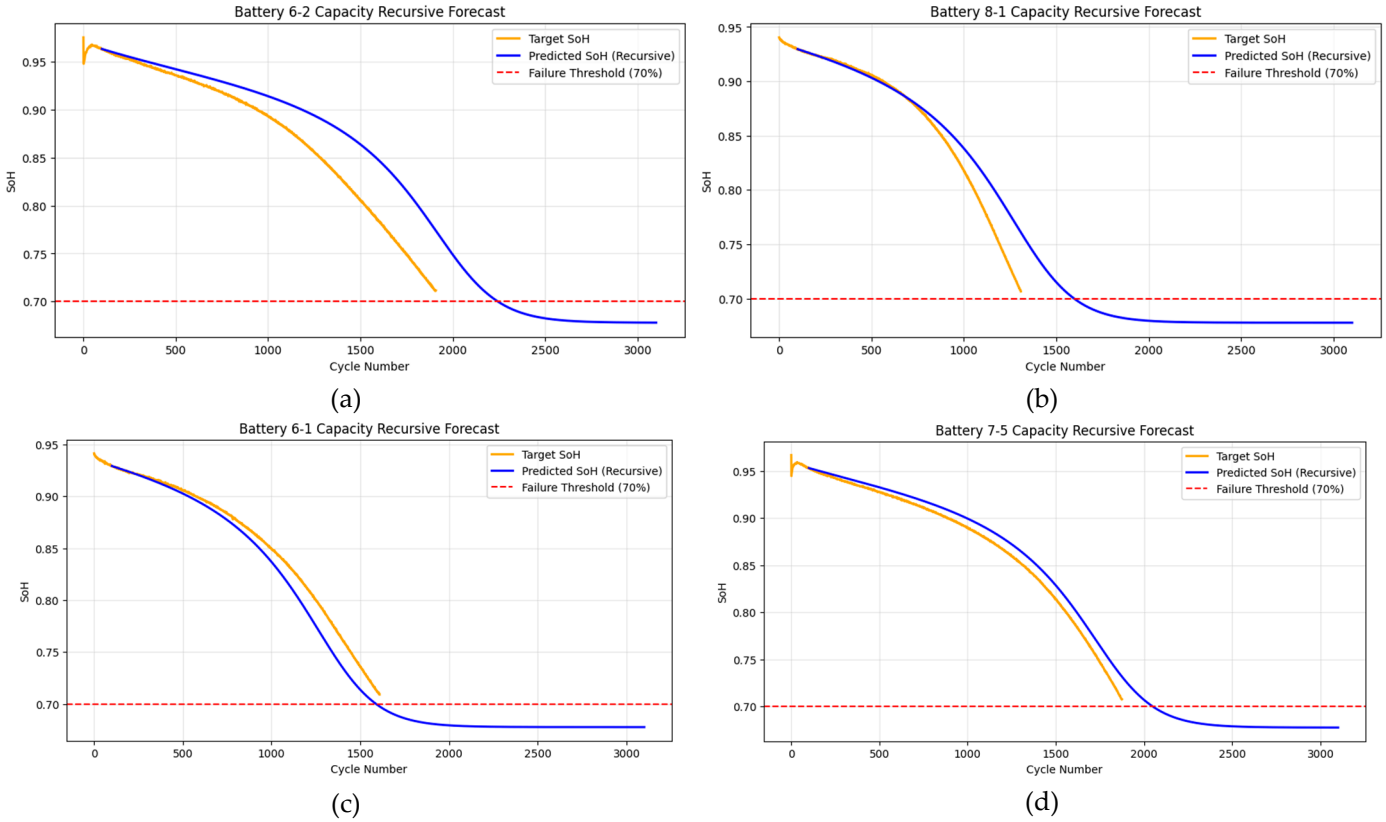

Figure 15. The target and predicted SoH curves from LSTM2 for cells 6-2 (a), 8-1 (b), 6-1 (c) and 7-5 (d).

5. Discussion

The evaluation of the Gompertz model, LSTM models and GILSTM models in Table 4 and Figure 14 provide meaningful insights into their individual strengths, weaknesses and applicability for RUL prediction of LFP batteries. The Gompertz model offered advantages in physical interpretability with its parameters found to be strongly correlated to RUL, making it a suitable choice for real-world applications where interpretability is crucial. The Gompertz model was found to have poor

© 2026 by the author(s). Distributed under a Creative Commons CC BY license.

Preprints.org (www.preprints.org) | NOT PEER-REVIEWED | Posted: 19 March 2026 doi:10.20944/preprints202603.1540.v1

standalone performance before cycle 1000 where RUL prediction is most valuable, with some RMSE values hitting a hundred thousand. These poor early-cycle stage results may be attributed to the erratic behaviour seen in Appendix A when the SoH is higher than 0.9. Below 0.9 SoH the Gompertz and its derivative functions are seen to stabilize into smoother curves explaining the superior performance in mid-cycle and late-cycle stages; the performance in these stages catches up to LSTM1 and LSTM2, the best models in this study. Despite the high early-cycle stage RMSEs of the Gompertz, when SoH curves are predicted accurately or are known such as in the Gompertz baseline, the performance was quite good with an RMSE of 27.9 cycles (1.4%). This indicates that the main issue may be intrinsic to SoH curve prediction. Note that some of that error can be attributed to the fact that none of the cells hit 0.7 SoH but the RUL prediction used 0.7, this was more of an error in the functioning of the electronic BMS.

The developed LSTM models (LSTM1 and LSTM2) captured the overall degradation trends and temporal dynamics of battery life without overfitting. These LSTMs had the best performance in this study and are comparable to the state-of-the-art models developed in other studies being only outperformed by BatLiNet [54] by a 3.4% margin. The developed GILSTM models (GILSTM1 and GILSTM2) were found to have overfit on the SoH data, with predictions of k, a and b centroiding to the mean values of the targets. GILSTM3 used the Gompertz and Inverse Gompertz functions to verify the RUL predictions of LSTM2. From Figure 14, the GILSTM3 model was found to be performing poorly in comparison to the developed baseline LSTM models as the error went up with increase in cycles. For all developed non-GILSTM models, RUL prediction was better in mid-cycle to late-cycle stages than in early-cycle stages suggesting limitations in early-cycle RUL prediction. The GILSTMs did not generalize, this might be due to the limited dataset size. While the conceptual basis for the integration of the Gompertz and the LSTM is sound, further optimization of the GILSTM is necessary to realize its full potential.

6. Conclusions

This study demonstrates that while data-driven and physics-based models offer distinct advantages for RUL prediction in LFP batteries, achieving high value interpretable hybrid integration remains a significant challenge. LSTM1 and LSTM2 emerged as the most accurate predictors capturing temporal dynamics without overfitting and performing within 3.4% of the best state-of-the-art models. The Gompertz model provided superior physical interpretability despite early-cycle instability when the SoH was above 0.9, its performance in later stages stabilized to get much closer to the top-performing LSTMs.

The Gompertz-Informed LSTMs failed to bridge the gap between data-driven and physics-based models, underperforming due to overfitting and a tendency for parameter predictions of k, a and b to centroid toward mean values. Future work should focus on battery dataset expansion and optimization of the development of parameter predicting PINN models.

Author Contributions: Conceptualization, Y.N., C.w.M. and E.M.; methodology, Y.N and C.w.M.; software, Y.N.; validation, C.w.M. and E.M.; formal analysis, Y.N.; investigation, Y.N.; data curation, Y.N.; writing—original draft preparation, Y.N.; writing—review and editing, Y.N., C.w.M. and E.M.; visualization, Y.N.; supervision, C.w.M. and E.M.; funding acquisition, C.w.M. All authors have read and agreed to the published version of the manuscript.

Funding: This work was conducted as part of the Artificial Intelligence for Development (AI4D) program, with the financial support of the UK government's Foreign, Commonwealth, and Development Office (FCDO) and Canada's International Development Research Centre (IDRC). In addition, we appreciate support from Arm and Google.org to DSAIL. This work was also supported by a grant from the Swiss National Supercomputing Centre (CSCS) under project ID g164 on Alps. Additional computational resources for modelling and benchmarking results were obtained through Kaggle.

Data Availability Statement: The data utilized in this study are available from three sources:.

© 2026 by the author(s). Distributed under a Creative Commons CC BY license.

Preprints.org (www.preprints.org) | NOT PEER-REVIEWED | Posted: 19 March 2026 doi:10.20944/preprints202603.1540.v1

(1) **HUST Battery Dataset**, a dataset for real-time personalized health status prediction of lithium-ion batteries using deep transfer learning, available at https://data.mendeley.com/datasets/nsc7hnsg4s/2, accessed on 30th August 2024;

(2) **The source code for this study is available at https://github.com/DeKUT-DSAIL/gi-lstms**

Acknowledgments: During the preparation of this study, the author(s) used Gemini 3 Pro for the purposes of troubleshooting programming bugs and aiding improved visualization of results. The authors have reviewed and edited the output and take full responsibility for the content of this publication.

Conflicts of Interest: The authors declare no conflicts of interest. The funders had no role in the design of the study; in the collection, analyses, or interpretation of data; in the writing of the manuscript; or in the decision to publish the results.

Abbreviations

The following abbreviations are used in this manuscript:

BESS	Battery Energy Storage System
BoL	Beginning of Life
BMS	Battery Management System
CC	Coulomb Counting
C_{rated}	Nominal Capacity/Rated Capacity
EoL	End of Life
EV	Electric Vehicle
GILSTM	Gompertz-Informed Long Short-Term Memory
kWh	Kilowatt hour
LFP	Lithium Iron Phosphate
LiB	Lithium-ion Battery
LSTM	Long Short-Term Memory
MSE	Mean Squared Error
NCA	lithium Nickel Cobalt Aluminium oxide
NMC	lithium Nickel Manganese Cobalt oxide
SAIDI	System Average Interruption Duration Index
SoC	State of Charge
SoH	State of Health
RMSE	Root Mean Squared Error
RUL	Remaining Useful Life
WS	Window Size

Appendix A

The Figure below shows the relationship between HUST SoH data and the Gompertz (y), the first derivative ($\frac{dy}{dx}$) and the second derivative.

© 2026 by the author(s). Distributed under a Creative Commons CC BY license.

Preprints.org (www.preprints.org) | NOT PEER-REVIEWED | Posted: 19 March 2026 doi:10.20944/preprints202603.1540.v1

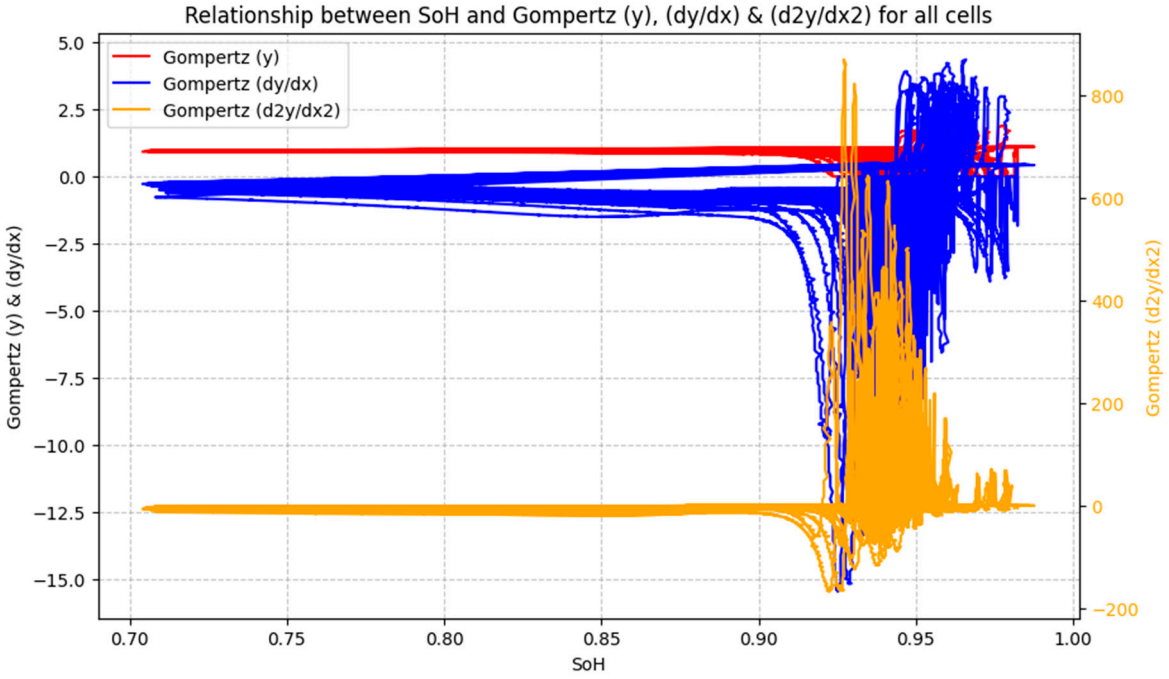

At SoH values between 0.90 and 1.0, the Gompertz (y), the first derivative ($\frac{dy}{dx}$) and the second derivative exhibit high variability while below 0.9 SoH, the curves smoothen out showing how in the initial SoH stages it is far harder to predict RUL and SoH based on the Gompertz function than in the latter stages, 0.9 SoH to 0.7 SoH.

References

1. 'Kenya Power Explains 5 Cause of Numerous Blackouts - Kenyans.co.ke'. Accessed: Jun. 11, 2025. [Online]. Available: https://www.kenyans.co.ke/news/112075-kenya-power-explains-5-cause-numerous-blackouts
2. K. M. U. Ahmed, M. Alvarez, and M. H. J. Bollen, 'Reliability Analysis of Internal Power Supply Architecture of Data Centers in Terms of Power Losses', *Electric Power Systems Research*, vol. 193, p. 107025, Apr. 2021, doi: 10.1016/j.epsr.2021.107025.
3. Y. S. Hussein *et al.*, 'Data Centre Infrastructure: Power Efficiency and Protection', in *Latest Advances and New Visions of Ontology in Information Science*, IntechOpen, 2023. doi: 10.5772/intechopen.110014.
4. L. Lin, R. Wijayawardana, V. Rao, H. Nguyen, E. W. Gnibga, and A. A. Chien, 'Exploding AI Power Use: an Opportunity to Rethink Grid Planning and Management', in *The 15th ACM International Conference on Future and Sustainable Energy Systems*, Singapore Singapore: ACM, Jun. 2024, pp. 434–441. doi: 10.1145/3632775.3661959.
5. E. Serban, M. Ordonez, and C. Pondiche, 'Voltage and Frequency Grid Support Strategies Beyond Standards', *IEEE Transactions on Power Electronics*, vol. 32, no. 1, pp. 298–309, Jan. 2017, doi: 10.1109/TPEL.2016.2539343.
6. B. Nzomo, 'Electricity Reliability Worsens as System Losses Hit 24.2% Amid Aging Grid', The Kenyan Wall Street - Business, Markets News, Investing Data & AI Tools. Accessed: Jun. 11, 2025. [Online]. Available: https://kenyanwallstreet.com/electricity-reliability-worsens-as-system-losses-hit-24-2-amid-aging-grid/
7. 'Kenya increases power connection to consumers | Energy'. Accessed: Jun. 11, 2025. [Online]. Available: https://energy.go.ke/kenya-increases-power-connection-consumers
8. 'World Bank BESS Project Disclosures'. Accessed: Jun. 16, 2025. [Online]. Available: https://www.kengen.co.ke/index.php/information-center/the-bess-project.html
9. X. Feng, D. Ren, and M. Ouyang, 'Safety of lithium battery materials chemistry', *Journal of Materials Chemistry A*, vol. 11, no. 46, pp. 25236–25246, 2023, doi: 10.1039/D3TA04182D.
10. G. Wei *et al.*, 'A comprehensive insight into the thermal runaway issues in the view of lithium-ion battery intrinsic safety performance and venting gas explosion hazards', *Applied Energy*, vol. 349, p. 121651, Nov. 2023, doi: 10.1016/j.apenergy.2023.121651.

© 2026 by the author(s). Distributed under a Creative Commons CC BY license.

Preprints.org (www.preprints.org) | NOT PEER-REVIEWED | Posted: 19 March 2026 doi:10.20944/preprints202603.1540.v1

11. W. Li, H. Wang, Y. Zhang, and M. Ouyang, 'Flammability characteristics of the battery vent gas: A case of NCA and LFP lithium-ion batteries during external heating abuse', *Journal of Energy Storage*, vol. 24, p. 100775, Aug. 2019, doi: 10.1016/j.est.2019.100775.
12. M. Brand *et al.*, 'Electrical safety of commercial Li-ion cells based on NMC and NCA technology compared to LFP technology', in *2013 World Electric Vehicle Symposium and Exhibition (EVS27)*, Nov. 2013, pp. 1–9. doi: 10.1109/EVS.2013.6914893.
13. 'Watt Happens Next: LFP is Taking Over — Here's Why It Matters', ERV. Accessed: Apr. 14, 2025. [Online]. Available: https://erv.io/knowledge_hub/watt-happens-next-lfp-is-taking-over-heres-why-it-matters/
14. J. Mou *et al.*, 'Prediction of the Remaining Useful Life of Lithium-Ion Batteries Based on the 1D CNN-BLSTM Neural Network', *Batteries*, vol. 10, no. 5, Apr. 2024, doi: 10.3390/batteries10050152.
15. R. Shekhar, 'Comprehensive Compilation of Energy Units and Conversion Factors: A Technical Reference', Sep. 2024.
16. C. R. Lashway and O. A. Mohammed, 'Adaptive Battery Management and Parameter Estimation Through Physics-Based Modeling and Experimental Verification', *IEEE Transactions on Transportation Electrification*, vol. 2, no. 4, pp. 454–464, Dec. 2016, doi: 10.1109/TTE.2016.2558843.
17. B. Sundén, 'Chapter 6 - Thermal management of batteries', in *Hydrogen, Batteries and Fuel Cells*, B. Sundén, Ed., Academic Press, 2019, pp. 93–110. doi: 10.1016/B978-0-12-816950-6.00006-3.
18. X. Kong, A. Bonakdarpour, B. T. Wetton, D. P. Wilkinson, and B. Gopaluni, 'State of Health Estimation for Lithium-Ion Batteries', *IFAC-PapersOnLine*, vol. 51, no. 18, pp. 667–671, Jan. 2018, doi: 10.1016/j.ifacol.2018.09.347.
19. R. Xiong, H. He, F. Sun, and K. Zhao, 'Evaluation on State of Charge Estimation of Batteries With Adaptive Extended Kalman Filter by Experiment Approach', *IEEE Transactions on Vehicular Technology*, vol. 62, no. 1, pp. 108–117, Jan. 2013, doi: 10.1109/TVT.2012.2222684.
20. Y. Zhang, W. Song, S. Lin, and Z. Feng, 'A novel model of the initial state of charge estimation for LiFePO4 batteries', *Journal of Power Sources*, vol. 248, pp. 1028–1033, Feb. 2014, doi: 10.1016/j.jpowsour.2013.09.135.
21. F. Feng, R. Lu, and C. Zhu, 'A Combined State of Charge Estimation Method for Lithium-Ion Batteries Used in a Wide Ambient Temperature Range', *Energies*, vol. 7, no. 5, Art. no. 5, May 2014, doi: 10.3390/en7053004.
22. A. Gailani, R. Mokidm, M. El-Dalahmeh, M. El-Dalahmeh, and M. Al-Greer, 'Analysis of Lithium-ion Battery Cells Degradation Based on Different Manufacturers', Jul. 03, 2020, *arXiv*: arXiv:2007.01937. doi: 10.48550/arXiv.2007.01937.
23. M. Witczak, M. Mrugalski, and B. Lipiec, 'Remaining Useful Life Prediction of MOSFETs via the Takagi–Sugeno Framework', *Energies*, vol. 14, no. 8, p. 2135, Jan. 2021, doi: 10.3390/en14082135.
24. J.-Y. Wu, M. Wu, Z. Chen, X.-L. Li, and R. Yan, 'Degradation-Aware Remaining Useful Life Prediction With LSTM Autoencoder', *IEEE Transactions on Instrumentation and Measurement*, vol. 70, pp. 1–10, 2021, doi: 10.1109/TIM.2021.3055788.
25. M. G. Alfarizi, B. Tajiani, J. Vatn, and S. Yin, 'Optimized Random Forest Model for Remaining Useful Life Prediction of Experimental Bearings', *IEEE Transactions on Industrial Informatics*, vol. 19, no. 6, pp. 7771–7779, Jun. 2023, doi: 10.1109/TII.2022.3206339.
26. S. Sayyad, S. Kumar, A. Bongale, P. Kamat, S. Patil, and K. Kotecha, 'Data-Driven Remaining Useful Life Estimation for Milling Process: Sensors, Algorithms, Datasets, and Future Directions', *IEEE Access*, vol. 9, pp. 110255–110286, 2021, doi: 10.1109/ACCESS.2021.3101284.
27. Y. Zhou, C. Liu, X. Yu, B. Liu, and Y. Quan, 'Tool wear mechanism, monitoring and remaining useful life (RUL) technology based on big data: a review', *SN Appl. Sci.*, vol. 4, no. 8, p. 232, Jul. 2022, doi: 10.1007/s42452-022-05114-9.
28. A. Ayob, S. Ansari, M. S. H. Lipu, A. Hussain, and M. H. M. Saad, 'SOC, SOH and RUL Estimation for Supercapacitor Management System: Methods, Implementation Factors, Limitations and Future Research Improvements', *Batteries*, vol. 8, no. 10, p. 189, Oct. 2022, doi: 10.3390/batteries8100189.
29. K. Manmi, M. Tuchel, E. Kendrick, and F. Brosa Planella, 'A Comparison of Standard SEI Growth Models in the Context of Battery Formation', *J. Electrochem. Soc.*, vol. 171, no. 10, p. 100530, Oct. 2024, doi: 10.1149/1945-7111/ad8548.

© 2026 by the author(s). Distributed under a Creative Commons CC BY license.

Preprints.org (www.preprints.org) | NOT PEER-REVIEWED | Posted: 19 March 2026 doi:10.20944/preprints202603.1540.v1

30. H. Adenusi, G. A. Chass, S. Passerini, K. V. Tian, and G. Chen, 'Lithium Batteries and the Solid Electrolyte Interphase (SEI)—Progress and Outlook', *Advanced Energy Materials*, vol. 13, no. 10, p. 2203307, 2023, doi: 10.1002/aenm.202203307.
31. M. Frankenberger *et al.*, 'SEI Growth Impacts of Lamination, Formation and Cycling in Lithium Ion Batteries', *Batteries*, vol. 6, no. 2, p. 21, Jun. 2020, doi: 10.3390/batteries6020021.
32. S. Hosseininasab, C. Lin, S. Pischinger, M. Stapelbroek, and G. Vagnoni, 'State-of-health estimation of lithium-ion batteries for electrified vehicles using a reduced-order electrochemical model', *Journal of Energy Storage*, vol. 52, p. 104684, Aug. 2022, doi: 10.1016/j.est.2022.104684.
33. L. D. Couto, O. Capron, J. Servotte, R. Ponnette, and G. Mulder, 'Physics-based lifetime modeling and parameter identification of lithium-ion batteries under various degradation conditions', *Journal of Energy Storage*, vol. 127, p. 116739, Aug. 2025, doi: 10.1016/j.est.2025.116739.
34. G. Ma *et al.*, 'Real-time personalized health status prediction of lithium-ion batteries using deep transfer learning', *Energy & Environmental Science*, vol. 15, no. 10, pp. 4083–4094, 2022, doi: 10.1039/D2EE01676A.
35. K. A. Severson *et al.*, 'Data-driven prediction of battery cycle life before capacity degradation', *Nat Energy*, vol. 4, no. 5, pp. 383–391, May 2019, doi: 10.1038/s41560-019-0356-8.
36. M. Catelani, L. Ciani, R. Fantacci, G. Patrizi, and B. Picano, 'Remaining Useful Life Estimation for Prognostics of Lithium-Ion Batteries Based on Recurrent Neural Network', *IEEE Transactions on Instrumentation and Measurement*, vol. 70, pp. 1–11, 2021, doi: 10.1109/TIM.2021.3111009.
37. H. Feng and G. Shi, 'SOH and RUL prediction of Li-ion batteries based on improved Gaussian process regression', *J. Power Electron.*, vol. 21, no. 12, pp. 1845–1854, Dec. 2021, doi: 10.1007/s43236-021-00318-5.
38. G. Cheng, X. Wang, and Y. He, 'Remaining useful life and state of health prediction for lithium batteries based on empirical mode decomposition and a long and short memory neural network', *Energy*, vol. 232, p. 121022, Oct. 2021, doi: 10.1016/j.energy.2021.121022.
39. Y. Ma, M. Yao, H. Liu, and Z. Tang, 'State of Health estimation and Remaining Useful Life prediction for lithium-ion batteries by Improved Particle Swarm Optimization-Back Propagation Neural Network', *Journal of Energy Storage*, vol. 52, p. 104750, Aug. 2022, doi: 10.1016/j.est.2022.104750.
40. S. Wang, Y. Fan, S. Jin, P. Takyi-Aninakwa, and C. Fernandez, 'Improved anti-noise adaptive long short-term memory neural network modeling for the robust remaining useful life prediction of lithium-ion batteries', *Reliability Engineering & System Safety*, vol. 230, p. 108920, Feb. 2023, doi: 10.1016/j.ress.2022.108920.
41. Y. Li, L. Kang, X. Wang, D. Xie, and S. Wang, 'State of Health Prediction of Lithium-Ion Batteries Based on Dual-Time-Scale Self-Supervised Learning', *Batteries*, vol. 11, no. 8, p. 302, Aug. 2025, doi: 10.3390/batteries11080302.
42. X. Li *et al.*, 'A Physics-Guided Transformer for Robust State of Charge Estimation in Aging Lithium-Ion Batteries', *Batteries*, vol. 11, no. 12, Dec. 2025, doi: 10.3390/batteries11120446.
43. S. S. Madani *et al.*, 'Artificial Intelligence and Digital Twin Technologies for Intelligent Lithium-Ion Battery Management Systems: A Comprehensive Review of State Estimation, Lifecycle Optimization, and Cloud-Edge Integration', *Batteries*, vol. 11, no. 8, p. 298, Aug. 2025, doi: 10.3390/batteries11080298.
44. H. Zhang, X. Gui, S. Zheng, Z. Lu, Y. Li, and J. Bian, 'BATTERYML: AN OPEN-SOURCE PLATFORM FOR MA- CHINE LEARNING ON BATTERY DEGRADATION', 2024.
45. C. P. Winsor, 'The Gompertz Curve as a Growth Curve', *Proceedings of the National Academy of Sciences*, vol. 18, no. 1, pp. 1–8, Jan. 1932, doi: 10.1073/pnas.18.1.1.
46. N. Yang, Z. Song, H. Hofmann, and J. Sun, 'Robust State of Health estimation of lithium-ion batteries using convolutional neural network and random forest', *Journal of Energy Storage*, vol. 48, p. 103857, Apr. 2022, doi: 10.1016/j.est.2021.103857.
47. Y. Che, X. Hu, X. Lin, J. Guo, and R. Teodorescu, 'Health prognostics for lithium-ion batteries: mechanisms, methods, and prospects', *Energy Environ. Sci.*, vol. 16, no. 2, pp. 338–371, Feb. 2023, doi: 10.1039/D2EE03019E.
48. B. M. E. Ph.D, 'What are Battery Management Systems and How do they Impact Energy Storage Systems?', AZoM. Accessed: Mar. 03, 2025. [Online]. Available: https://www.azom.com/article.aspx?ArticleID=22797

© 2026 by the author(s). Distributed under a Creative Commons CC BY license.

Preprints.org (www.preprints.org) | NOT PEER-REVIEWED | Posted: 19 March 2026 doi:10.20944/preprints202603.1540.v1

49. M. M. Ur Rehman *et al.*, 'Modular approach for continuous cell-level balancing to improve performance of large battery packs', in *2014 IEEE Energy Conversion Congress and Exposition (ECCE)*, Sep. 2014, pp. 4327–4334. doi: 10.1109/ECCE.2014.6953991.
50. H. Bašić, V. Bobanac, and H. Pandžić, 'Determination of Lithium-Ion Battery Capacity for Practical Applications', *Batteries*, vol. 9, no. 9, Sep. 2023, doi: 10.3390/batteries9090459.
51. S. Hochreiter and J. Schmidhuber, 'Long Short-Term Memory', *Neural Comput.*, vol. 9, no. 8, pp. 1735–1780, Nov. 1997, doi: 10.1162/neco.1997.9.8.1735.
52. D. P. Kingma and J. Ba, 'Adam: A Method for Stochastic Optimization', Jan. 30, 2017, *arXiv*: arXiv:1412.6980. doi: 10.48550/arXiv.1412.6980.
53. M. Raissi, P. Perdikaris, and G. E. Karniadakis, 'Physics-informed neural networks: A deep learning framework for solving forward and inverse problems involving nonlinear partial differential equations', *Journal of Computational Physics*, vol. 378, pp. 686–707, Feb. 2019, doi: 10.1016/j.jcp.2018.10.045.
54. H. Zhang *et al.*, 'Accurate battery lifetime prediction across diverse aging conditions with deep learning', Nov. 24, 2023, *arXiv*: arXiv:2310.05052. doi: 10.48550/arXiv.2310.05052.

Disclaimer/Publisher's Note: The statements, opinions and data contained in all publications are solely those of the individual author(s) and contributor(s) and not of MDPI and/or the editor(s). MDPI and/or the editor(s) disclaim responsibility for any injury to people or property resulting from any ideas, methods, instructions or products referred to in the content.

© 2026 by the author(s). Distributed under a Creative Commons CC BY license.